THE ASTROPHYSICAL JOURNAL, 474:223–255, 1997 January 1

DESTRUCTION OF THE GALACTIC GLOBULAR CLUSTER SYSTEM

OLEG Y. GNEDIN AND JEREMIAH P. OSTRIKER
Princeton University Observatory, Peyton Hall, Princeton, NJ 08544; ognedin@astro.princeton.edu, jpo@astro.princeton.edu
Received 1996 February 15; accepted 1996 July 24

ABSTRACT

We investigate the dynamical evolution of the Galactic globular cluster system in considerably greater detail than has been done hitherto, finding that destruction rates are significantly larger than given by previous estimates. The general scheme (but not the detailed implementation) follows Aguilar, Hut, & Ostriker.

For the evolution of individual clusters, we use a Fokker-Planck code including the most important physical processes governing the evolution: two-body relaxation, tidal truncation of clusters, compressive gravitational shocks while clusters pass through the Galactic disk, and tidal shocks due to passage close to the bulge. Gravitational shocks are treated comprehensively, using a recent result by Kundić & Ostriker that the $\langle \Delta E^2 \rangle$ shock-induced relaxation term, driving an additional dispersion of energies, is generally more important than the usual energy shift term $\langle \Delta E \rangle$. Various functional forms of the correction factor are adopted to allow for the adiabatic conservation of stellar actions in a presence of transient gravitational perturbation.

We use a recent compilation of the globular cluster positional and structural parameters, and a collection of radial velocity measurements. Two transverse to the line-of-sight velocity components were assigned randomly according to the two kinematic models for the cluster system (following the method of Aguilar, Hut, & Ostriker): one with an isotropic peculiar velocity distribution, corresponding to the present-day cluster population, and the other with the radially preferred peculiar velocities, similar to those of the stellar halo. We use the Ostriker & Caldwell and the Bahcall, Schmidt, & Soneira models for our Galaxy.

For each cluster in our sample, we calculated its orbits over a Hubble time, starting from the *present* observed positions and assumed velocities. Medians of the resulting set of peri- and apogalactic distances and velocities are used then as an input for the Fokker-Planck code. Evolution of the cluster is followed up to its total dissolution due to a coherent action of all of the destruction mechanisms. The rate of destruction is then obtained as a median over all the cluster sample, in accord with Aguilar, Hut, & Ostriker.

We find that the total destruction rate is much larger than that given by Aguilar, Hut, & Ostriker with more than half of the present clusters (52%–58% for the Ostriker & Caldwell model, and 75%–86% for the Bahcall, Schmidt, & Soneira model) destroyed in the next Hubble time. Alternatively put, the typical time to destruction is comparable to the typical age, a result that would follow from (but is not required by) an initially power law distribution of destruction times. We discuss some implications for a past history of the globular cluster system and the initial distribution of the destruction times, raising the possibility that the current population is but a very small fraction of the initial population with the remnants of the destroyed clusters constituting presently a large fraction of the spheroid (bulge + halo) stellar population.

Subject headings: celestial mechanics, stellar dynamics — Galaxy: kinematics and dynamics — globular clusters: general

1. INTRODUCTION

Globular clusters are thought to be the oldest stellar systems in our Galaxy, and a history of attempts by theoreticians and observers to understand the keys of their evolution is as old as the discipline of stellar dynamics, with a comprehensive review provided by Spitzer (1987). Yet, these relatively simple stellar systems are not understood well enough to predict their future with desirable accuracy, in part due to lack of accurate observational values for the current dynamical state and in part due to a residual uncertainty concerning the complete catalog of relevant physical processes operating on these systems. More than that, we have almost no clues about their past, and in particular, whether what we see now is representative of the *initial* globular cluster system, or just a small leftover after a great destruction battle that occurred earlier in the history of the Galaxy. In this paper we consider the evolution of the globular clusters and their ultimate disappearance and propose a simple model for their initial distribution.

Pre– and post–core collapse evolution of an isolated cluster is relatively well understood (Spitzer 1987; Goodman 1993). Significant progress in understanding of the evolution was achieved using Monte Carlo and Fokker-Planck calculations. But the galactic environment makes the clusters subject to external perturbations—tidal truncation and the gravitational shocks due to passages close to the bulge and through the disk. The shock processes, although known to be important, have never been carefully included in the evolution of the system. We investigate the Fokker-Planck models including the shocks elsewhere (Gnedin, Lee, & Ostriker 1997a, hereafter GLO) and show that the dispersion of energy of the stars, induced by the shocks (Kundić & Ostriker 1995, hereafter KO), is generally even more important for the evolution than the first-order

energy shift. Another very important aspect of modeling globular clusters is the initial mass spectrum. Multimass clusters undergo core collapse much faster than in the single-mass case, and their destruction is much more efficient (see Lee & Goodman 1995, and the references in GLO). We restrict ourselves, however, to the single-mass models in order to maintain clear physical understanding, but owing to omission of this aspect of the problem, our results provide a lower bound to the rate of destruction of the globular clusters.

As long as we have (at least, an approximate) understanding of the evolution of a single cluster, we can turn to the study of the system of globular clusters in our Galaxy and in external galaxies. Chernoff, Kochanek, & Shapiro (1986) used a semianalytical Monte Carlo technique to estimate the importance of the different mechanisms acting upon the cluster. They considered two-body relaxation, tidal stripping of stars, and the first-order tidal shocking effect—due to the disk crossing and interactions with giant molecular clouds (GMCs). For each of those processes, they calculated the cluster mass and energy changes associated with them to predict the evolution. They followed the cluster evolution only up to core collapse and assumed a single-mass King model (King 1966) for the internal structure of the cluster. Tidal heating due to the GMCs was found to be negligible compared to the disk shocks. Note, however, that the Galactic model assumed in that work (Bahcall, Schmidt, & Soneira 1983, hereafter BSS) is strongly favorable to the disk shock for the clusters with small galactocentric radius since the surface density of the disk increases exponentially as the radius decreases (see § 2.2). Chernoff et al. (1986) concluded that many of the clusters located within inner 3 kpc from the Galactic center have undergone core collapse and that many of them may already have been destroyed. A number of authors have pointed out that the bulge and stellar spheroid themselves could be composed of remnants of the destroyed globular clusters, if prior destruction of globular clusters occurred at high enough rate.

Another mechanism for the mass loss is stellar evolution. Chernoff & Shapiro (1987) used a method similar to that of Chernoff et al. (1986) and included a power-law initial mass function for the cluster stars. Mass loss due to stellar evolution is important for the early evolution of the cluster but then fades away because the mass loss is large only for massive stars whose lifetime is short. Comprehensive study including the effects of stellar evolution has been done by Chernoff & Weinberg (1990). They used a Fokker-Planck code with an extensive spectrum of stellar masses (20 species), which includes stellar evolution and relaxation processes. Multimass models evolve much faster, and the evaporation rate is larger. Also, mass segregation (Spitzer 1987) speeds up core collapse. Mass loss during first 5×10^9 yr is sufficiently strong to disrupt weakly concentrated clusters ($c < 0.6$). Combined with the relaxation, it destroys many low-mass and low-concentration clusters within a Hubble time.

The present characteristics and the evolutionary state of the observed Galactic globular clusters were also investigated by Aguilar, Hut, & Ostriker (1988, hereafter AHO). We will draw heavily on that paper and compare our results with AHO. AHO used a sample of the 83 Galactic globular clusters with known structural parameters and line-of-sight velocities. They considered virtually all the important physical mechanisms (except the mass spectrum and mass loss due to stellar evolution) to calculate the present-day destruction rates for the clusters in the sample. The rates were defined as the inverse time it takes for a given mechanism to dissolve a cluster, in units of a Hubble time, which is nominally defined as 10^{10} yr. They estimated the rates for evaporation through the tidal boundary, disk and bulge tidal shocks, and dynamical friction. The last process has not been widely investigated in its application for the cluster evolution. Its effect reduces to gradual spiraling of the cluster toward the Galactic center, as the cluster loses orbital energy owing to continuous interactions with field stars and dark halo. AHO found that this mechanism is a relatively unimportant one, except for unusually massive clusters. They calculated a number of orbits associated with each cluster in the sample and took a median over the whole resulting distribution for a corresponding destruction rate. They investigated two galactic models (Ostriker & Caldwell 1983, hereafter OC and BSS; § 2.2) and two kinematic models for the globular cluster system: isotropic, which corresponds to the current distribution, and predominantly radial, which resembles that of the halo stars and which might be closer to an *initial* cluster distribution. The assumption concerning the velocity distribution is necessary as only one velocity component is observed. (Note that the program to obtain true space velocities of globular clusters is underway; Cudworth & Hanson 1993). We discuss the kinematic models in § 2.3.

The central bulge was found to be very efficient in destroying clusters on highly elongated orbits. This leads to an *isotropization* of the orbits and even preferential survival of tangentially biased orbits in the Hubble time. Thus, an initially radial distribution better fits the present population than the initially isotropic one. At the current time, evaporation is the most important destruction process. The difference between the two galactic models was found to be relatively small, except for the disk shocking that obviously depends on the body of the surface mass profile. AHO introduced a weighting factor that accounts for the fact that some orbits are less probable because of the various destruction mechanisms acting upon the cluster. Such a weighting reduces the computed rates but converges to a similar value of 0.05 for all galactic models and kinematic profiles considered. This implies that only four or five clusters are destroyed over a Hubble time for the present conditions. But AHO treated clusters in a simplified fashion as King models, and they (like other investigators) did not allow for the tidal shock relaxation phenomena. It is these defects that we remedy in the present paper.

Long, Ostriker, & Aguilar (1992) investigated the effect of the bar in our Galaxy on the destruction of the globular clusters. Barred orbits can bring the clusters close to the Galactic center where they are efficiently destroyed. However, only a small increase in the destruction rate was detected. Therefore, we did not consider the bar in this work.

Finally, a recent paper by Hut & Djorgovski (1992) used a statistical approach and approximate analytical estimates for the relaxation times for a sample of 140 clusters. They concluded that the current evaporation rate is 5 ± 3 Gyr^{-1} (about 10 times the rate found by AHO), which means that a significant fraction of the present-day clusters would be destroyed in the next Hubble time.

In this paper we make a significant improvement over AHO by applying detailed Fokker-Planck calculations to

the globular cluster sample. We describe the sample in § 2.1 and the galactic models in § 2.2. Then we discuss the two kinematic models and compare the resulting properties of the orbits for our sample. In § 2.5, we describe the destruction mechanisms involved in the globular cluster evolution. We conclude § 2 with the history of our code and the formulation of the numerical strategy. Section 3 presents our results for all runs. Finally, we speculate on the possible past history and future fate of the Galactic globular clusters in § 4. Section 5 sums up our conclusions.

2. METHOD

2.1. *Observational Data*

We have used a recent compilation of globular cluster coordinates by Djorgovski & Meylan (1993) and distances and absolute magnitudes from Djorgovski (1993). Cluster concentrations, core radii, and half-mass radii were taken from Trager, Djorgovski, & King (1993). The core-collapsed clusters were assigned a limiting concentration of $c = 2.5$. We used a constant mass-to-light ratio to obtain the cluster masses, $(M/L)_V = 3$ in solar units (Djorgovski 1993).

We selected 119 clusters of 143 with available photometric data. All clusters in our sample have measured radial velocities, which we collected from several sources. Cudworth & Hanson (1993) have derived actual space velocities for 14 clusters, but we chose not to use those data to maintain homogeneity of the sample. We assign two unknown velocity components to each cluster using our statistical method in § 2.3.

The observed parameters of our sample are given in Table 1. The first two columns are the sequential number and cluster's name. The next two columns are the Galactic coordinates. D is the distance of the cluster from the Sun in kiloparsecs, and R is the galactocentric radius. The seventh column is concentration $c = \log (R_t/R_c)$, followed by core radius R_c in parsecs. Tidal radius R_t was calculated from the previous two quantities. The next column is the cluster mass converted from its luminosity. The last two columns are the line-of-sight velocities and the reference numbers to various sources. The references are listed in at the end of Table 1.

2.2. *Galactic Model*

To evaluate the gravitational shocks on the clusters we have used two models for our Galaxy: the OC model D-150, and the BSS model. AHO present a detailed comparison between the two models. In the OC model, the disk is represented as the difference of two exponentials that vanishes at the center, whereas BSS's disk density rises monotonically as R decreases. The BSS model has also a compact nuclear component within 1 central kpc. Thus, both disk and bulge shocks (§ 2.5) are expected to be more prominent for the BSS model. As suggested by AHO, we consider the difference of the results for the two models as a measure of uncertainty associated with the distribution of mass within the Galaxy.

We use the same routine to compute the Galactic model as was done by AHO. The routine was kindly provided to us by L. Aguilar.

2.3. *Velocity Distribution for the Globular Cluster System*

Kinematic models for the Galactic globular cluster system (GCS) have been sought widely in the past (see, e.g., Frenk & White 1980; Thomas 1989). Frenk & White (1980) studied a sample of 66 clusters and found no evidence for the radial expansion of the GCS as a whole. Their best fit to observed kinematic distribution is that with the isotropic velocity dispersion rising with the galactocentric distance as $R^{0.2}$. An isotropic and isothermal (with constant velocity dispersion) model is still consistent with their data at the 90% confidence level. Later work by Thomas (1989) included 115 clusters and confirmed the absence of the expansion. He found that within the inner 7 kpc to the Galactic center, the velocity distribution is isotropic, but for the outer radii, the velocity ellipsoid with slightly increasing line-of-sight dispersion may be preferred. Rotation velocity estimates and line-of-sight velocity dispersions as well as their errors for both sources are given in Table 2.

We repeated the analysis of the velocity distribution using our sample. We adopted the solar motion relative to the LSR of $(-9, 12, 7)$ km s^{-1} (Mihalas & Binney 1981, p. 400) and the circular velocity of the LSR of 220 km s^{-1}. Line-of-sight projections of the two velocities were subtracted from the observed radial velocities to obtain v_r relative to an inertial frame. Then the rotation velocity and its uncertainty were estimated using equations (15) and (16) of Thomas (1989). After subtraction of the rotation velocity along the line of sight, we end up with the peculiar velocities with (presumably) zero mean. Both our $v_{\rm rot}$ and $\sigma_{\rm los}$ are in agreement with the above results within errors. Our adopted values are also summarized in Table 2.

Following AHO we investigate two *initial* kinematic models for the globular cluster system. The first has an isotropic peculiar velocity distribution with constant velocity dispersion. This is the simplest model still consistent with the observations. We used the one-dimensional dispersion of 118 km s^{-1}, resulting from our sample.

The second model is anisotropic with velocity ellipsoid axis ratio at solar position $r_\odot = 8.5$ kpc similar to the spheroid stellar Population II:

$$\frac{\sigma_r^2}{\sigma_t^2} = 1 + \frac{r^2}{r_a^2}, \tag{1}$$

where σ_r and σ_t are the one-dimensional dispersions radial and transverse to the Galactic center, respectively. We have adopted the AHO value of the anisotropy radius $r_a = (0.8)^{1/2}\, r_\odot \approx 7.6$ kpc. Cluster orbits for this distribution are nearly isotropic within r_a and become more and more radial with increasing distance from the center.

The amplitude of the radial velocity dispersion can be obtained from the Jeans equation for the constant circular velocity potential. Integration of the Jeans equation in spherical coordinates gives (see, e.g., Ogorodnikov 1965)

$$\frac{d\rho\sigma_r^2}{dr} + \frac{\rho}{r}\,(2\sigma_r^2 - 2\sigma_t^2 - v_{\rm rot}^2) = -\rho\,\frac{v_{\rm circ}^2}{r}. \tag{2}$$

For the velocity ellipsoid given by equation (1) and the power-law density profile $\rho \propto r^{-\alpha}$, we obtain

$$\sigma_r^2 = (v_{\rm circ}^2 - v_{\rm rot}^2)\,\frac{[r^2/(\alpha - 2)] + (r_a^2/\alpha)}{r^2 + r_a^2}. \tag{3}$$

We accept $v_{\rm circ} = 220$ km s^{-1} as the standard value for the circular velocity. Thomas (1989) found $\alpha = 3.5$ for his

TABLE 1

GLOBULAR CLUSTER PARAMETERS

ID	Name	l (deg)	b (deg)	D (kpc)	R (kpc)	c	R_c (pc)	R_t (pc)	M ($M_\odot$)	V_r (km s^{-1})	References
1	NGC 0104	305.90	−44.89	4.6	7.8	2.04	0.50	54.8	1.45e+06	−19.0	1
2	NGC 0288	152.28	−89.38	8.3	11.9	0.96	3.47	31.6	1.11e+05	−46.0	1
3	NGC 0362	301.53	−46.25	8.5	9.6	1.94	0.43	37.5	3.78e+05	223.2	1
4	NGC 1261	270.54	−52.13	15.9	18.0	1.27	1.82	33.9	3.26e+05	51.0	2
5	Pal 1	130.07	19.03	13.7	20.1	1.50	0.60	19.0	2.54e+03	3.0	2
6	AM 1	258.36	−48.47	124.7	126.1	1.23	4.57	77.6	1.81e+04	116.0	3
7	Eridanus	218.11	−41.33	79.5	84.8	1.10	5.89	74.2	2.30e+04	−21.0	3
8	Pal 2	170.53	−9.07	13.6	21.9	1.40	0.60	15.1	1.74e+05	−133.0	3
9	NGC 1851	244.51	−35.04	12.3	17.3	2.24	0.28	48.7	5.61e+05	320.5	1
10.....	NGC 1904	227.23	−29.35	12.9	19.2	1.72	0.60	31.5	3.57e+05	203.4	1
11.....	NGC 2298	245.63	−16.01	10.0	15.5	1.28	1.00	19.1	7.20e+04	150.4	5
12.....	NGC 2419	180.37	25.24	83.2	91.0	1.40	8.51	213.8	1.60e+06	−20.0	1
13.....	NGC 2808	282.19	−11.25	9.1	11.1	1.77	0.71	41.8	1.32e+06	98.0	2
14.....	Pal 3	240.14	41.86	90.3	93.8	1.00	12.59	125.9	6.38e+04	84.0	2
15.....	NGC 3201	277.23	8.64	5.1	9.3	1.31	2.09	42.7	1.95e+05	494.6	1
16.....	Pal 4	202.31	71.80	98.2	101.0	0.78	15.85	95.5	5.41e+04	75.0	2
17.....	NGC 4147	252.85	77.19	18.7	21.0	1.80	0.55	34.7	6.69e+04	183.0	1
18.....	NGC 4372	300.99	−9.88	5.2	7.4	1.30	2.63	52.5	3.20e+05	49.0	2
19.....	Rup 106	300.89	11.67	19.7	17.1	0.70	5.75	28.8	8.42e+04	−44.0	6
20.....	NGC 4590	299.63	36.05	9.3	9.8	1.64	1.86	81.2	3.06e+05	−95.1	1
21.....	NGC 4833	303.61	−8.01	5.8	7.2	1.25	1.70	30.2	9.49e+04	194.0	2
22.....	NGC 5024	332.96	79.77	18.5	19.1	1.78	2.00	120.5	7.33e+05	−80.0	2
23.....	NGC 5053	335.69	78.94	16.1	16.9	0.82	10.47	69.2	1.66e+05	42.8	1
24.....	NGC 5139	309.10	14.97	4.9	6.8	1.24	3.72	64.6	2.64e+06	232.2	1
25.....	NGC 5272	42.21	78.71	10.2	12.3	1.85	1.48	104.8	7.82e+05	−146.7	1
26.....	NGC 5286	311.61	10.57	9.3	7.4	1.46	0.78	22.5	4.80e+05	57.1	1
27.....	NGC 5466	42.15	73.59	15.8	16.3	1.43	8.91	239.8	1.33e+05	107.2	1
28.....	NGC 5634	342.21	49.26	25.1	20.9	1.60	1.51	60.1	2.86e+05	−41.9	2
29.....	NGC 5694	331.06	30.36	32.8	27.0	1.84	0.59	40.8	2.92e+05	−142.8	1
30.....	IC 4499	307.35	−20.47	18.9	15.7	1.11	5.37	69.2	1.66e+05	41.0	7
31.....	NGC 5824	332.56	22.07	32.7	26.2	2.45	0.52	146.6	8.98e+05	−26.1	1
32.....	Pal 5	0.85	45.86	23.1	18.3	0.74	19.50	107.2	2.84e+04	−56.0	8
33.....	NGC 5897	342.95	30.29	12.5	7.3	0.79	7.24	44.6	2.00e+05	102.9	3
34.....	NGC 5904	3.86	46.80	7.5	6.5	1.87	0.89	66.0	8.34e+05	53.9	1
35.....	NGC 5927	326.60	4.86	8.0	4.8	1.60	0.98	39.0	3.71e+05	−106.0	2
36.....	NGC 5946	327.58	4.19	10.4	5.6	2.50	0.23	72.7	5.66e+05	129.0	1
37.....	NGC 5986	337.02	13.27	10.2	4.6	1.22	1.91	31.7	4.98e+05	94.0	2
38.....	Pal 14	28.75	42.18	73.0	67.7	0.72	23.44	123.0	2.00e+04	72.0	4
39.....	NGC 6093	352.67	19.46	8.5	3.1	1.95	0.36	32.1	3.67e+05	7.7	1
40.....	NGC 6101	317.75	−15.82	14.9	10.7	0.80	5.01	31.6	1.32e+05	364.3	5
41.....	NGC 6121	350.97	15.97	2.0	6.6	1.59	0.49	19.1	2.25e+05	70.9	2
42.....	NGC 6144	351.93	15.70	9.9	3.2	1.30	2.69	53.7	1.52e+05	162.0	2
43.....	NGC 6139	342.37	6.94	9.1	3.0	1.80	0.35	22.1	4.18e+05	4.0	2
44.....	NGC 6171	3.37	23.01	6.4	3.6	1.51	1.00	32.4	2.04e+05	−34.0	1
45.....	NGC 6205	59.01	40.91	7.1	8.7	1.49	1.82	56.2	6.27e+05	−246.4	1
46.....	NGC 6218	15.72	26.31	5.5	4.7	1.38	1.07	25.7	4.93e+05	−42.6	1
47.....	NGC 6229	73.64	40.31	31.6	30.9	1.61	1.23	50.1	4.46e+05	−154.2	10
48.....	NGC 6235	358.92	13.52	9.6	2.4	1.33	1.00	21.4	1.71e+05	86.0	2
49.....	NGC 6254	15.14	23.08	4.3	5.1	1.40	1.07	26.9	2.25e+05	75.5	1
50.....	NGC 6256	347.79	3.31	10.2	2.7	2.50	0.07	22.1	7.68e+04	−104.7	1
51.....	Pal 15	18.87	24.30	41.3	34.2	0.60	14.45	57.5	2.74e+04	68.9	1
52.....	NGC 6266	353.57	7.32	5.6	3.1	1.70	0.29	14.5	8.98e+05	−71.9	1
53.....	NGC 6273	356.87	9.38	10.9	2.9	1.53	1.35	45.7	1.56e+06	131.0	2
54.....	NGC 6284	358.35	9.94	11.8	3.8	2.50	0.25	79.1	2.17e+05	27.4	1
55.....	NGC 6287	0.13	11.02	6.7	2.3	1.60	0.52	20.7	1.03e+05	−208.0	2
56.....	NGC 6293	357.62	7.83	8.4	1.2	2.50	0.11	34.8	2.34e+05	−148.0	1
57.....	NGC 6304	355.83	5.38	6.0	2.7	1.80	0.36	22.7	1.93e+05	−98.0	10
58.....	NGC 6316	357.18	5.76	12.8	4.5	1.55	0.62	22.0	1.02e+06	76.0	2
59.....	NGC 6325	0.97	8.00	6.0	2.7	2.50	0.05	15.8	9.57e+04	30.9	1
60.....	NGC 6341	68.34	34.86	7.5	9.5	1.81	0.51	32.9	3.64e+05	−120.5	10
61.....	NGC 6333	5.54	10.71	7.4	2.0	1.15	1.26	17.8	2.89e+05	224.7	10
62.....	NGC 6342	4.90	9.72	12.1	4.1	2.50	0.16	50.6	1.95e+05	117.9	1
63.....	NGC 6356	6.72	10.22	16.6	8.5	1.54	1.12	38.8	8.19e+05	31.6	10
64.....	NGC 6355	359.58	5.43	7.0	1.7	2.50	0.10	31.6	3.67e+05	−184.0	2
65.....	NGC 6352	341.42	−7.17	6.1	3.5	1.10	1.48	18.6	1.22e+05	−118.0	2
66.....	NGC 6366	18.41	16.04	4.0	5.1	0.92	2.14	17.8	3.92e+04	−122.6	1
67.....	NGC 6362	325.56	−17.57	7.8	5.4	1.10	2.95	37.1	1.17e+05	−13.3	1
68.....	NGC 6388	345.56	−6.74	11.0	3.7	1.70	0.40	20.0	1.50e+06	77.0	2
69.....	NGC 6402	21.32	14.80	10.1	4.4	1.60	2.45	97.5	1.23e+06	−123.4	10
70.....	NGC 6401	3.45	3.98	6.3	2.3	1.69	0.45	22.0	1.23e+06	−62.0	2
71.....	NGC 6397	338.17	−11.96	2.2	6.5	2.50	0.03	9.5	1.59e+05	17.7	1
72.....	NGC 6426	28.09	16.23	17.5	11.3	1.70	1.35	67.7	9.49e+04	−162.0	2

TABLE 1—*Continued*

ID	Name	l (deg)	b (deg)	D (kpc)	R (kpc)	c	R_c (pc)	R_t (pc)	M ($M_\odot$)	V_r (km s^{-1})	References
73	NGC 6440	7.73	3.80	7.1	1.8	1.70	0.26	13.0	5.72e+05	−83.0	2
74	NGC 6441	353.53	−5.00	10.7	2.5	1.85	0.35	24.8	1.30e+06	16.0	1
75	NGC 6453	355.72	−3.87	10.1	1.8	2.50	0.20	63.2	1.32e+05	−84.0	2
76	NGC 6496	348.02	−10.01	5.8	3.3	0.70	1.74	8.7	4.63e+04	−95.0	2
77	NGC 6517	19.23	6.76	6.1	3.5	1.82	0.11	7.3	1.82e+05	−37.0	2
78	NGC 6522	1.02	−3.93	7.2	1.4	2.50	0.11	34.8	5.93e+04	−10.4	1
79	NGC 6535	27.18	10.44	7.0	4.1	1.30	0.83	16.6	5.93e+04	−215.3	1
80	NGC 6528	1.14	−4.17	6.6	2.0	2.29	0.17	33.1	9.31e+04	160.0	2
81	NGC 6539	20.80	6.78	4.0	5.0	1.60	0.63	25.1	1.60e+05	−52.0	2
82	NGC 6544	5.84	−2.20	2.6	5.9	2.50	0.03	9.5	1.30e+05	−12.0	10
83	NGC 6541	349.29	−11.18	6.7	2.7	2.00	0.58	58.0	4.67e+05	−152.8	10
84	NGC 6553	5.25	−3.02	3.6	4.9	1.17	0.56	8.3	2.61e+05	−24.0	2
85	NGC 6558	0.20	−6.03	8.9	1.0	2.50	0.09	28.5	2.41e+05	−198.9	1
86	NGC 6569	0.48	−6.68	8.8	1.0	1.27	0.95	17.7	3.85e+05	−26.0	2
87	NGC 6584	342.14	−16.41	9.5	3.9	1.20	1.66	26.3	2.19e+05	180.0	10
88	NGC 6624	2.79	−7.91	8.1	1.3	2.50	0.15	47.4	3.32e+05	54.2	1
89	NGC 6626	7.80	−5.58	6.0	2.8	1.67	0.42	19.6	4.42e+05	15.5	1
90	NGC 6638	7.90	−7.15	8.4	1.6	1.40	0.65	16.3	1.12e+05	−14.0	10
91	NGC 6637	1.72	−10.27	10.2	2.4	1.39	1.00	24.5	3.44e+05	50.1	10
92	NGC 6642	9.81	−6.44	7.9	1.8	1.99	0.24	23.5	1.26e+05	−47.0	2
93	NGC 6652	1.53	−11.38	14.3	6.2	1.80	0.30	18.9	2.59e+05	−124.2	10
94	NGC 6656	9.89	−7.55	3.0	5.6	1.31	1.23	25.1	5.36e+05	−148.8	11
95	Pal 8	14.11	−6.80	28.6	20.6	0.75	3.31	18.6	2.21e+05	−38.0	12
96	NGC 6681	2.85	−12.51	9.2	2.1	2.50	0.07	22.1	1.89e+05	221.1	1
97	NGC 6712	25.35	−4.32	6.8	3.8	0.90	1.86	14.8	2.45e+05	−107.5	1
98	NGC 6715	5.61	−14.09	21.1	13.1	1.84	0.66	45.7	1.45e+06	142.0	5
99	NGC 6717	12.88	−10.90	7.3	2.6	2.07	0.18	21.1	1.23e+05	−6.0	2
100.....	NGC 6723	0.07	−17.30	8.6	2.6	1.05	2.40	26.9	3.74e+05	−79.0	2
101.....	NGC 6752	336.50	−25.63	4.2	5.5	2.50	0.21	66.4	3.64e+05	−32.1	1
102.....	NGC 6760	36.11	−3.92	6.1	5.1	1.59	0.59	23.0	1.38e+05	−28.0	2
103.....	Terzan 7	3.39	−20.07	36.7	28.9	1.08	6.46	77.7	6.15e+04	162.0	13
104.....	NGC 6779	62.66	8.34	9.7	9.6	1.37	1.05	24.6	1.89e+05	−135.9	1
105.....	Arp 2	8.55	−20.79	28.2	20.6	0.90	13.18	104.7	3.26e+04	119.0	13
106.....	NGC 6809	8.79	−23.27	4.8	4.6	0.76	3.98	22.9	2.41e+05	175.5	1
107.....	Terzan8	5.76	−24.56	23.0	15.7	0.60	6.61	26.3	2.50e+04	130.0	13
108.....	Pal 11	31.80	−15.58	13.2	7.9	0.69	7.76	38.0	1.38e+05	−68.0	10
109.....	NGC 6838	56.74	−4.56	3.9	7.2	1.15	0.72	10.2	3.67e+04	−23.0	1
110.....	NGC 6864	20.30	−25.75	18.7	12.4	1.88	0.51	38.7	4.89e+05	−195.2	10
111.....	NGC 6934	52.10	−18.89	14.8	12.0	1.53	1.07	36.3	2.15e+05	−412.2	1
112.....	NGC 6981	35.16	−32.68	18.1	13.7	1.23	2.82	47.9	1.81e+05	−309.0	2
113.....	NGC 7006	63.77	−19.41	38.8	36.1	1.42	2.75	72.3	2.52e+05	−364.0	2
114.....	NGC 7078	65.01	−27.31	10.4	10.7	2.50	0.21	66.4	9.84e+05	−107.1	14
115.....	NGC 7089	53.38	−35.78	11.8	10.7	1.80	1.17	73.8	8.81e+05	−3.1	1
116.....	NGC 7099	27.18	−46.84	7.4	7.1	2.50	0.12	37.9	2.74e+05	−185.7	1
117.....	Pal 12	30.51	−47.68	19.1	15.8	0.90	6.17	49.0	2.02e+04	28.5	15
118.....	Pal 13	87.10	−42.70	24.5	25.6	1.00	2.82	28.2	5.12e+03	13.0	16
119.....	NGC 7492	53.39	−63.48	25.0	24.2	1.00	6.17	61.7	5.56e+04	−188.5	10

REFERENCES.—(1) Pryor & Meylan 1993 (in case of multiple choice, mean values are assumed); (2) Hesser, Shawl, & Meyer 1986; (3) Suntzeff, Olszewski, & Stetson 1985; (4) Zaritsky et al. 1989; (5) Geisler et al. 1995; (6) Da Costa, Armandroff, & Norris 1992; (7) Cannon 1993; (8) Schweitzer, Cudworth, & Majewski 1993; (9) Peterson, Rees, & Cudworth 1995; (10) Webbink 1981; (11) Peterson, & Cudworth 1994; (12) Zinn & West 1984; (13) Da Costa & Armandroff 1995; (14) Peterson, Seitzer, & Cudworth 1989; (15) Armandroff & Da Costa 1991; (16) Kulessa & McDowell 1985.

sample of globular clusters. In this paper we assume $\alpha = 3$, corresponding to the old spheroid stellar population.

TABLE 2

KINEMATIC PARAMETERS OF GALACTIC GLOBULAR CLUSTER SYSTEM

References	$v_{\rm rot}$ (km s^{-1})	$\sigma_{\rm los}$ (km s^{-1})
Frenk & White 1980.....	60 ± 26	118 ± 20[a]
Thomas 1989	65 ± 18	110 ± 7
This paper	60 ± 21	119 ± 39

[a] The uncertainty of the velocity dispersion is taken as an average over radial bins of Table 1 from White & Frenk 1983.

The distribution of peculiar velocities at a given galactocentric position r of a cluster is then (AHO, eq. [4])

$$f(v_r, v_{t1}, v_{t2}) = A \exp\left(-\frac{v_r^2}{2\sigma_r^2} - \frac{v_{t1}^2 + v_{t2}^2}{2\sigma_t^2}\right), \qquad (4)$$

where v_r is the radial galactocentric velocity, and v_{t1}, v_{t2} are the two transverse components. Note that this form of the distribution function is a modification of an isothermal sphere and is an *Ansatz*, since the Jeans equation describes only the variance of the actual distribution function. We use equation (4) only to complement the two unknown velocity components.

The distribution of orbital eccentricities is shown in

Figures 1 and 2 for the OC and BSS models, respectively. The upper panels in both figures show histograms for the anisotropic velocity ellipsoids, and the lower ones show histograms for the isotropic distribution. Note how the number of large eccentricities changes from the former to the latter.

2.4. *Orbit Integration*

In order to model the gravitational shocks experienced by a cluster flying by the Galactic center (bulge shock), we need an estimate of a perigalacticon distance $R_{\rm peri}$ and an orbit shape (eccentricity e) for each cluster from our sample. We use the orbit integration routine described in AHO, which employs a fourth-order Runge-Kutta method with variable time step. The Galactic model extends up to a distance of 250 kpc, and all orbits beyond that point are discarded.

Only four of the needed six phase space parameters required to start the calculation of orbits are known from the observations (Table 1): three spatial coordinates and a velocity component along the line of sight. To complement the two "missing" tangential velocities, we used a statistical approach similar to that of AHO. The two velocities were randomly drawn and then selected using the rejection method (Press et al. 1992, p. 290) in order for the total three-dimensional peculiar velocity be consistent with the assumed kinematic model (§ 2.3). The systemic rotation velocity was then added to the peculiar velocity, and the resulting velocity with respect to the Galactic center was used for the orbit integration.

We have followed trajectories that each cluster makes in 10 billion years. Perigalactic and apogalactic distances were calculated as medians from the set of all orbits. Similarly, we determine the velocity of the cluster at the perigalacticon (which we use to calculate the amplitude of the bulge shock; § 2.5.3) and the vertical velocity component at the point where the cluster crosses the disk (to estimate the strength of the disk shock; § 2.5.2). This set of the orbital parameters is used to calculate the strength of the tidal shocks on the cluster (§ 2.5).

Only one set of the parameters was used to reduce the amount of computations. We have checked that the final results do not change significantly if we use a different set of initial velocities and therefore different shock parameters, as long as they are consistent with the chosen galactic and kinematic models. These test runs for the OC model with the isotropic velocity distribution are reported in § 3.3.

Once chosen, the orbital parameters (R_p, R_a, V_p, V_z) of the clusters are fixed in the Fokker-Planck calculations. The actual amount of heating of the clusters changes, however, as the clusters evolve. As described in §§ 2.5.2 and 2.5.3, the changes in energy and energy squared depend on the internal velocity dispersion and size of the clusters. The assumption of the fixed orbital elements is justified if the galactic potential does not change—the cluster stars follow approximately same trajectories even when the cluster is destroyed as a self-gravitating system.

In contrast to AHO, we could not follow every orbit of the cluster because of the nature of the Fokker-Planck calculations. The code has its time step controlled by relaxation processes, and it seems hard to reconcile with the orbit integration procedure. We plan to return to this subject in our next paper and to try to perform simultaneous Fokker-Planck and orbital calculations that would allow us to model the evolution of the clusters in a more natural way.

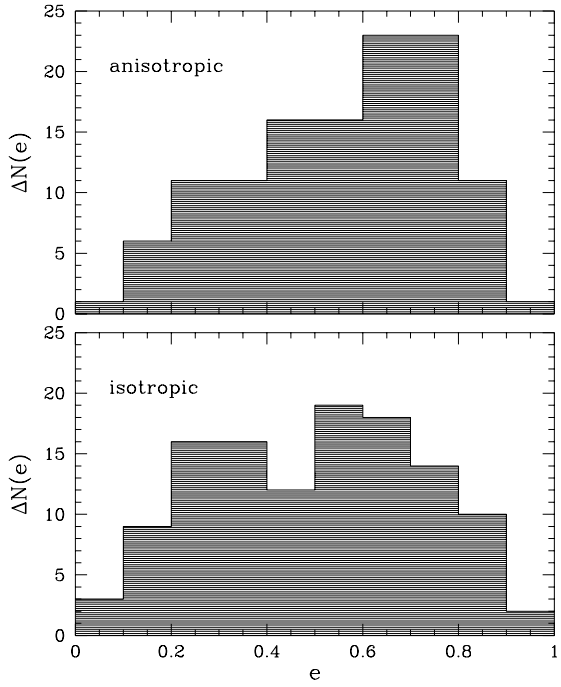

FIG. 1.—Histogram of the orbit eccentricity distribution in the OC galactic model, for the isotropic and anisotropic kinematic models.

2.5. *Dynamical Processes*

2.5.1. *Evaporation*

Two-body relaxation leads to escape of stars approaching the unbound tail of the cluster velocity distribution (Ambartsumian 1938; Spitzer 1940). Tidal truncation due to the Galactic potential accelerates this process. Much more dramatic effects result from the gravothermal instability, when the inner part of cluster contracts (core collapse) and the envelope expands. This, in turn, accelerates the rate of evaporation of stars from the cluster. A recent review of pre– and post–core collapse evolution of a tidally truncated cluster is given by Goodman (1993).

It is conventional to express the lifetime of a cluster in terms of the half-mass relaxation time (Spitzer & Hart 1971)

$$t_{\rm rh} \equiv 0.138 \frac{M^{1/2} R_h^{3/2}}{G^{1/2} m_* \ln(\Lambda)}, \tag{5}$$

where M is the total cluster mass, R_h is the half-mass radius, m_* is the average stellar mass, and $\ln(\Lambda) = \ln(0.4N)$ is the Coulomb logarithm, N being the number of stars in the cluster. Hénon (1961) introduced the "escape probability"

$$\xi_e \equiv -\frac{t_{\rm rh}}{M}\frac{dM}{dt}. \tag{6}$$

Here dM/dt is the mass-loss rate due to two-body relaxation. For the self-similar solutions, Hénon found $\xi_e \approx 0.045$. See GLO for a detailed discussion of the evaporation timescale.

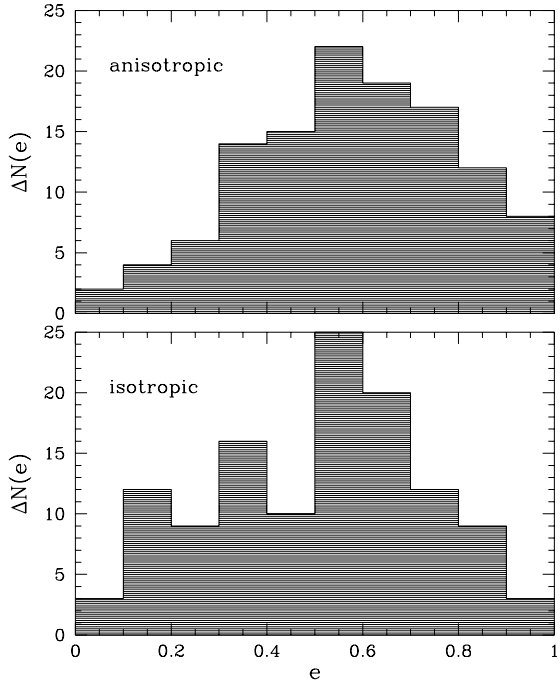

FIG. 2.—Histogram of the orbit eccentricity distribution in the BSS galactic model, for the isotropic and anisotropic kinematic models.

2.5.2. *Disk Shock*

When a cluster passes through the Galactic disk, it experiences a time-varying gravitational force that is pulling the cluster toward the equatorial plane. The characteristic timescale for this force is the time it takes the cluster to cross two vertical scale heights of the disk, H:

$$t_{\rm cross} \equiv \frac{2H}{V_z}\,, \tag{7}$$

and V_z is the cluster velocity component perpendicular to the Galactic plane. Because of the large orbital velocity of the cluster and the relatively small vertical extent of the disk, the crossing time is usually shorter than the orbital period of stars in the outer part of the cluster. Owing to the short-term nature of the effect, it was called a "compressive gravitational shock" (Ostriker, Spitzer, & Chevalier 1972). On average, stars gain energy, and the cluster binding energy is reduced. This accelerates the escape of stars from the cluster through evaporation.

On the other hand, in the central region of the cluster, the effect of the compressive shock is largely damped, since the stars move very fast and their orbits become adiabatically invariant. The impact of the shock is thus a strong function of position of a star inside the cluster. Following Spitzer (1987), we define an *adiabatic parameter*

$$x_d \equiv \frac{2\omega H}{V_z}\,, \tag{8}$$

where ω is the angular velocity of stars inside cluster (assuming for simplicity circular motions), and the subscript d stands for disk; x_d represents the ratio of the shock duration to the orbital period of a star, so that for small values of ω, the term "shock" is appropriate.

To evaluate quantitatively the effect of the disk shock, several approaches have been proposed in the literature. The simplest one, the impulse approximation, assumes that the shock is so fast that the stars do not change their positions in the cluster significantly over the crossing time $t_{\rm cross}$. However, for the reason of conservation of adiabatic invariants, this approximation highly overestimates the impact when $x_d \gtrsim 1$. A more careful treatment is given by the harmonic potential approximation (Spitzer 1958), where we assume all stars, initially at same radial distance r from the center of the cluster, move around the center with the same oscillation frequency ω. Then, referring to equation (25) of KO, the average energy shift for every star is

$$\langle \Delta E \rangle_{\rm disk} = \frac{2g_m^2 r^2}{3V_z^2} A_{d1}(x_d)\,, \tag{9}$$

where g_m is the maximum gravitational acceleration experienced by stars due to the disk. Here $A_{d1}(x_d)$ is the factor taking into account the adiabatic invariants. For the harmonic approximation (see, e.g., Spitzer 1987, eq. [5-28])

$$A_{d1}(x) = \exp\left(-\frac{x^2}{2}\right). \tag{10}$$

We refer to equation (10) as a *Spitzer correction.* However, recently Weinberg (1994a, 1994b, 1994c) showed that small perturbations of stellar orbits can still grow in a system with more than 1 degree of freedom. If the system is represented as a combination of multidimensional nonlinear oscillators, it is very likely that some of the perturbation frequencies will be commensurable with the oscillation frequencies of stars. Then those orbits receive a significant kick from the perturbation and thus no longer conserve their actions. Averaging over whole cluster can give an appreciable change in velocity and energy. Such resonances can occur even for an arbitrary small resonant mode. Consequently, the adiabatic factor $A_{d1}(x)$ is not exponentially small for large x but, rather, is a power law. The simplest form of the correction can be written as

$$A_{d1}(x) = \left(1 + \frac{x^2}{4}\right)^{-3/2}. \tag{11}$$

For large $x \gg 1$, $A_{d1} \propto x^{-3}$.[1] In the following, we call equation (11) the *Weinberg correction.* Figure 3 shows the difference between the two forms of the adiabatic correction. A much more detailed discussion of the Weinberg correction can be found in Gnedin et al. (1997b).

Besides the shift in energy of stars $\langle \Delta E \rangle$, the gravitational shock also induces a quadratic term $\langle \Delta E^2 \rangle$, which governs the dispersion of the energy spectrum and thus pushes some loosely bound stars outside the tidal radius, speeding the disassociation of the cluster. "Shock-induced relaxation" was mentioned briefly by Spitzer & Chevalier (1973; see also Spitzer 1987, p. 116[2]). Recently KO noted the importance of this effect. We refer the reader to that paper, in which it is shown that this tidal shock relaxation can be in many cases competitive with two-body relaxation in causing the evolution of a cluster. Like ordinary relaxation, it causes spread (diffusion) of initially similar orbits and ultimately tends to induce core collapse. The mass loss associated with the tidal shock relaxation was considered in the study by Chernoff et al. (1986). The regime when the

[1] This power-law index was suggested by S. Tremaine.

[2] We are indebted to L. Spitzer for pointing out this reference to us.

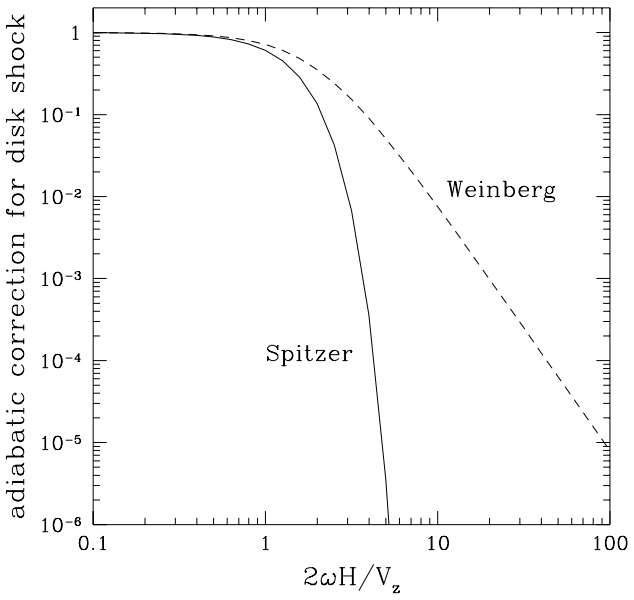

FIG. 3.—Comparison of the Spitzer (eq. [10]) and Weinberg (eq. [11]) adiabatic corrections for the disk shock, i.e., reductions in the energy change due to the shock because of the conservation of adiabatic invariants of stellar orbits inside the clusters vs. adiabatic parameter (eq. [8]).

shock-induced relaxation exceeds both the two-body rate and the first-order term, $\langle \Delta E \rangle$, has not been investigated before.

According to KO (their eq. [25])

$$\langle \Delta E^2 \rangle_{\rm disk} = \frac{4 g_m^2 \omega^2 r^4}{9 V_z^2} A_{d2}(x_d) , \tag{12}$$

where in the harmonic approximation

$$A_{d2}(x) = \frac{9}{5} \exp\left(-\frac{x^2}{2}\right) . \tag{13}$$

Note that the correction in this form does not match unity for $x \ll 1$. Rather, it goes a factor 1.8 over the impulse approximation. The harmonic potential obviously does not apply for the outer parts of the cluster, so some mismatch is expected. On the other hand, it enhances the shock in the cluster halo. We have chosen not to modify the Spitzer formula and to compare the calculations with those resulting from the Weinberg correction. The latter has been used in the same form of equation (11) for both energy terms. We have performed calculations with the two forms of the adiabatic correction and also a test case in the impulse regime (no correction was applied; $A_d \equiv 1$).

Disk shocks occur twice during the orbital period of the cluster, so we define the disk shock timescale at the half-mass radius (neglecting the adiabatic corrections) as

$$t_{\rm disk} \equiv \frac{P_{\rm orb}}{2} \left(\frac{-E}{\Delta E_h}\right) = \frac{3}{8} \left(\frac{V_z}{g_m}\right)^2 P_{\rm orb}\, \omega_h^2 , \tag{14}$$

where $P_{\rm orb}$ is the orbital period, $E \approx -0.2 GM/R_h$, and ΔE and ω are evaluated at R_h. Analogously, we find that

$$t_{\rm disk,2} \equiv \frac{P_{\rm orb}}{2} \left(\frac{E^2}{\Delta E_h^2}\right) = \frac{3}{4}\, t_{\rm disk} . \tag{15}$$

Both these terms contribute to the destruction of the cluster (although by quite different processes: $\langle \Delta E \rangle$ enhances evaporation and $\langle (\Delta E)^2 \rangle$ enhances core collapse), so that the total destruction rate associated with the disk shock may be written roughly as

$$\nu_{\rm disk} \equiv \frac{1}{t_{\rm disk}} + \frac{1}{t_{\rm disk,2}} = \frac{7}{3}\, t_{\rm disk}^{-1} . \tag{16}$$

2.5.3. *Bulge Shock*

Similar to the compressive disk shock, every globular cluster experiences a tidal shock during its passage close to the Galactic center. The massive compact component at the center of the Galaxy (bulge) induces a strong tidal force on the cluster near the perigalactic point of the cluster orbit. The difference between this effect and that from the smooth and steady tidal field of the Galaxy is primarily due to the time dependence of the bulge shock.

A very close effect of the tidal shock induced by giant molecular clouds was considered by L. Spitzer as early as 1958 (Spitzer 1958). The disturbing object was represented as a point mass, and the cluster orbit near the point of the closest approach (perigalacticon in our case) was assumed to be a straight path. Employing the harmonic approximation, we find the energy change for each star due to the bulge shock:

$$\langle \Delta E \rangle_{\rm bulge} = \frac{4}{3} \left(\frac{G M_b}{V_p R_p^2}\right)^2 r^2 A_{b1}(x_b) \chi(R_p) \lambda(R_p, R_a) . \tag{17}$$

Here M_b is the bulge mass, V_p is the cluster velocity at the perigalacticon R_p, and A_b is the corresponding adiabatic correction. Two new corrections arise as follows. The distribution of the bulge mass extends up to many kiloparsecs, and for some clusters it is not a good approximation to consider the bulge as a point mass. Rather, the tidal field exerted by such an extended mass profile will differ from the point-mass field (given by, e.g., Spitzer 1987). Details of the calculation of the correction factor $\chi(R_p)$ allowing for that effect will be given elsewhere (Gnedin & Hernquist 1997). We give here only the final expression that we use in our calculations:

$$\chi(R_p) = \tfrac{1}{2}[(3J_0 - J_1 - I_0)^2 + (2I_0 - I_1 - 3J_0 + J_1)^2 + I_0^2] , \tag{18}$$

where

$$I_0(R_p) \equiv \int_1^\infty m_b(R_p \zeta) \frac{d\zeta}{\zeta^2 (\zeta^2 - 1)^{1/2}} , \tag{19a}$$

$$I_1(R_p) \equiv \int_1^\infty \dot{m}_b(R_p \zeta) \frac{d\zeta}{\zeta^2 (\zeta^2 - 1)^{1/2}} , \tag{19b}$$

$$J_0(R_p) \equiv \int_1^\infty m_b(R_p \zeta) \frac{d\zeta}{\zeta^4 (\zeta^2 - 1)^{1/2}} , \tag{19c}$$

$$J_1(R_p) \equiv \int_1^\infty \dot{m}_b(R_p \zeta) \frac{d\zeta}{\zeta^4 (\zeta^2 - 1)^{1/2}} , \tag{19d}$$

and $m_b(R) \equiv M_b(R)/M_b$ is the normalized bulge mass distribution at radius R, with $\dot{m}_b(R) = dm_b(R)/d\ln R$.

Aguilar & White (1985; also AHO) proposed a correction of the form $\chi = \frac{1}{2} I_0^2$ only. Obviously that correction factor is everywhere smaller than ours (eq. [18]), although the difference is not dramatic. More importantly, it is different from the naive approximation when all the mass inside a radius R is taken to be a point-mass. The correction for the OC and BSS galactic models is illustrated in Figure 4.

The second correction, λ, is intended to take into account

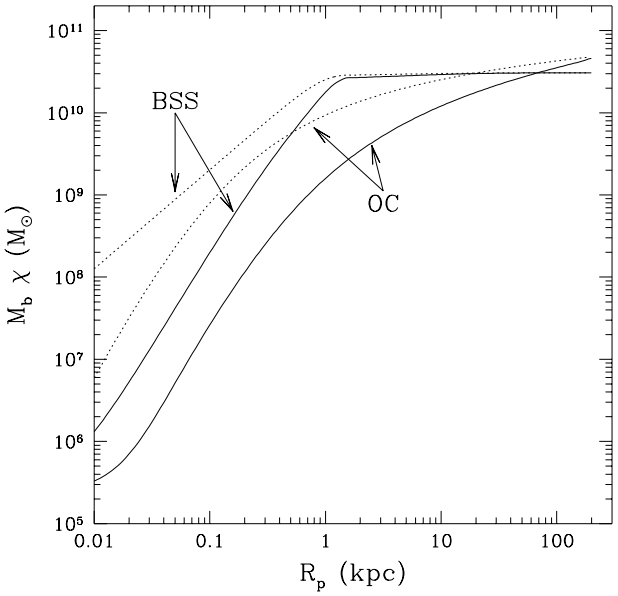

FIG. 4.—Correction factors vs. perigalactic distance for the bulge shock energy change due to the extended mass distribution for the bulge. Our correction ([eq. [18]) is shown by a solid curve, and that following from the point-mass approximation is shown as dots.

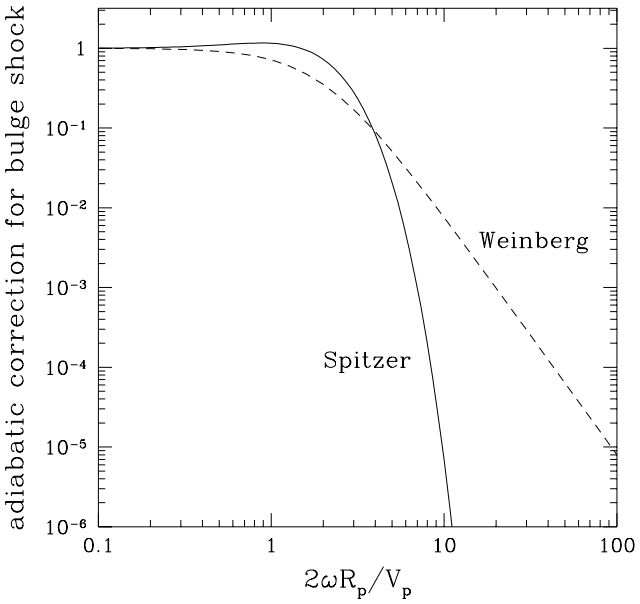

FIG. 5.—Same as Fig. 3, but for the bulge shock. The adiabatic parameter is given by eq. (21).

the time variation of the tidal force along an elliptic orbit of a cluster. Following AHO, we take the difference of the magnitudes of the tidal force at perigalacticon and apogalacticon as the total amplitude of the tidal effect. Thus the correction factor λ can be expressed as (AHO, eq. [11])

$$\lambda(R_p, R_a) = \left[1 - \frac{M_b(R_a)}{M_b(R_p)}\left(\frac{R_p}{R_a}\right)^3\right]^2 , \qquad (20)$$

where R_p and R_a are the perigalactic and apogalactic distances of the cluster, respectively.

Finally, $A_{b1}(x)$ is the corresponding adiabatic correction for the bulge shock. In the harmonic approximation we get the *Spitzer correction*: $A_{b1}(x) = \frac{1}{2}[L_x(x) + L_y(x) + L_z(x)]$ in his notation (Spitzer 1958, eqs. [36]–[38]). The *Weinberg correction* for the bulge shock was assumed to have the same functional form as for the disk shock (eq. [11]). The argument of the function A is now different,

$$x_b = \frac{2\omega R_p}{V_p} . \qquad (21)$$

Figure 5 compares the two corrections.

As in the case of the disk shock, the bulge shock induces the second-order relaxation term

$$\langle \Delta E^2 \rangle_{\rm bulge} = \frac{8}{9}\left(\frac{GM_b}{V_p R_p^2}\right)^2 \omega^2 r^4 A_{b2}(x_b)\chi(R_p)\lambda(R_p, R_a) . \qquad (22)$$

Analogously to the disk case, $A_{b2} = 9/5A_{b1}$ in the Spitzer regime, and $A_{b2} = A_{b1}$ for the Weinberg correction.

Similarly we define the bulge shock timescale. In this case, however, the effect occurs only once per cluster orbital period:

$$t_{\rm bulge} \equiv P_{\rm orb}\left(\frac{-E}{\Delta E_h}\right) = \frac{3}{8}\left(\frac{V_p R_p^2}{GM_b}\right)^2 P_{\rm orb}\,\omega_h^2 . \qquad (23)$$

$$t_{\rm bulge,2} \equiv P_{\rm orb}\left(\frac{E^2}{\Delta E_h^2}\right) = \frac{3}{4}\,t_{\rm bulge} . \qquad (24)$$

Finally, the total destruction rate associated with the bulge shock is

$$\nu_{\rm bulge} \equiv \frac{1}{t_{\rm bulge}} + \frac{1}{t_{\rm bulge,2}} = \frac{7}{3}\,t_{\rm bulge}^{-1} . \qquad (25)$$

2.6. *Fokker-Planck Code*

We calculate the dynamical evolution of the globular clusters from our sample using an orbit-averaged Fokker-Planck code descended from that of Cohn (1979, 1980). The code has been modified by Lee & Ostriker (1987) and Lee, Fahlman, & Richer (1991) to include a tidal boundary and three-body binary heating. Although the code allows a multicomponent stellar mass function, we restricted ourselves in this paper to a single-component case ($m_* = 0.7\ m_\odot$). This requires less parametrization of the numerical models and, we hope, gives clearer understanding of the physical processes involved. In the future, it certainly will be of interest to generalize the present calculations, including a realistic mass function. Lee & Goodman (1995), for example, considered evaporation of a multimass cluster in a steady tidal field and found that the mass loss doubles compared to the single-component case.

The tidal limit is determined by equating density inside the cluster to the Galactic density at a given point. Stars beyond the tidal boundary are not lost instantaneously but rather follow a continuous distribution function $f(\mathrm{E})$, as described in Lee & Ostriker (1987). This takes into account the fact that the tidal radius is not a strict "border" for the cluster because the internal force just balances the Galactic tidal force at that point. Therefore, the outer stars escape only when they go farther away from the cluster. The tidal field of the Galaxy is assumed to be steady and spherically symmetric. The latter is a weakness of a one-dimensional code (for further discussion, see GLO). The former assumption is valid only for a circular orbit of the cluster. For the actual elliptical orbit the maximum tidal stress occurs close to the perigalactic point and probably determines the tidal cutoff radius. A theoretical estimate for R_t is given by

Innanen, Harris, & Webbink (1983), who assumed a spherical mass distribution that increases linearly with galactocentric radius.

$$R_t = \frac{2}{3}\,[1 - \ln(1-e)]^{-1/3}\left[\frac{M_{cl}}{M_G(R_p)}\right]^{1/3} R_p\,, \qquad (26)$$

where e is eccentricity of the orbit, $e \equiv (R_a - R_p)/(R_a + R_p)$, R_a and R_p are the apogalactic and perigalactic points, respectively, and $M_G(R_p)$ is the galactic mass enclosed within R_p. However, proper calculation of the tidal radius is still a challenge for dynamicists, including its definition itself. For our calculations we used the observed *present-day* tidal radii (Table 1), which were obtained by fitting a single-mass King model to the observed cluster density profiles.

Heating of stars, reversing the core collapse, is due to three-body binaries. They are included explicitly, without following their actual formation and evolution, according to the prescription by Cohn (1985). Although Ostriker (1985) showed that the tidally captured binaries are probably more dynamically important for massive clusters than those formed through the three-body interactions, the reexpansion phase following the core collapse is largely independent of the central heating source (Henon 1961; Goodman 1993).

The implementation of the tidal shocks in the Fokker-Planck code deserves special attention, since it has not been done before. The orbit-averaged diffusion coefficients (Spitzer 1987) are modified to include the first- and second-order energy change rates due to the shocks. Since the disk shocking occurs twice per cluster orbit, we define $\langle D(\Delta E)\rangle$ and $\langle D(\Delta E^2)\rangle$ as the first- and second-order energy changes (eqs. [9] and [12]) over $P_{\rm orb}/2$. Analogously are defined the diffusion coefficients for the bulge shock, with the only correction that the bulge shock occurs once per cluster orbit. More detailed explanation of the changes in the code are given in a subsequent paper (GLO).

2.7. *Philosophy of the Numerical Experiments*

Our goal in this paper is to investigate the importance of the different destruction processes on the overall evolution of the Galactic globular cluster system. We consider the evaporation process and the disk and bulge gravitational shocks. AHO also included the dynamical friction in their orbit integrations, but we cannot model this effect at the moment. We rely on the results of AHO that the dynamical friction is not an important destruction mechanism for most clusters *at the present time.*

Also, AHO evaluated the destruction rates for all of the mechanisms separately. Using the Fokker-Planck code, we could only investigate the effects together, acting simultaneously. We hope this brings the numerical simulations closer to the reality, since in the real clusters, all of these processes act coherently, thus "helping" each other. For example, the disk and bulge shock-induced relaxation (eqs. [12] and [22]) combines with the normal two-body relaxation and enhances the evaporation of stars through the tidal boundary.

Nevertheless, it is of prime interest to rank the processes in their role for the destruction of the clusters. In particular, AHO found that the bulge shock is more important mechanism than the disk shock. Also, the newly discovered tidal shock relaxation (KO) has never been used in the detailed calculations of globular cluster evolution. How important are these processes? We try to answer this question using a "reduction" approach. We perform several sets of runs of the Fokker-Planck code, increasing the number of the processes allowed to act upon the cluster. The magnitude of each effect can then be estimated by subtracting the results of the run without that effect from the results of the run including the effect. Since we do not expect the effects to add in a linear fashion, such an estimate will only approximately determine the strength of the effect. Thus we organized the following series: (0) evaporation only; (1) evaporation + disk shock, $\langle\Delta E\rangle$ term only, no tidal shock relaxation; (2) evaporation + disk shock, including the relaxation term $\langle\Delta E^2\rangle$; (3) evaporation + disk shock + bulge shock, without tidal shock relaxation; and finally (4) evaporation + disk shock + bulge shock, including the relaxation. The last run includes all the processes we consider in this paper and produces the total destruction rate for the globular clusters.

For each set of runs, we repeat the calculations 3 times, allowing for different adiabatic conservation factors for the shock processes (§§ 2.5.2 and 2.5.3). The first run includes the Spitzer correction, the second includes the Weinberg correction, and the last one assumes the impulse approximation with no adiabatic correction applied.

Each run includes the Fokker-Planck simulations for all of the clusters in our sample, starting from the present time and ending with their total destruction. We use the observed concentrations and core radii of the clusters (Table 1) to model their current structure, which we approximate by a single-mass King model. The statistically assigned kinematic parameters (R_p, R_a, V_z, V_p; § 2.4) were used to estimate the amplitude of the tidal shocks. We followed evolution of the cluster up to a late stage near total destruction when the code breaks down owing to numerical difficulties in recomputation the cluster potential. The remaining mass at that point is on average 8% (but no more than 11%) of the initial cluster mass. Destruction time t_d was extrapolated using the least-squares linear fit to the last 10 integration steps to a point of zero mass. This gives a more robust estimate of t_d than linear extrapolation from the last couple of points because many clusters suffer the gravothermal instability (see, e.g., Goodman 1993) at the late stages of their evolution. Real clusters will cease to exist as bound systems before $M_{\rm cl} = 0$, so that t_d is an overestimate of the actual destruction time and an underestimate of the destruction rate.

Given the destruction times for all the clusters in the sample, we define the destruction rate in units of a Hubble time

$$\nu \equiv \frac{t_{\rm Hubble}}{t_d} = \frac{10^{10}\ \rm yr}{t_d}\,. \qquad (27)$$

This definition agrees with the destruction rates of AHO, thus allowing a direct comparison. Since the resulting distribution of the rates is broad and in general asymmetric around the mean, we choose to take median $\tilde{\nu}$ of the sample as a characteristic value, in accordance with AHO. Also, a few clusters from the sample have $\nu \sim 10^3$ and therefore dominate in the mean and standard deviation. The standard error of the median was estimated as (Kendall, Stuart, & Ord 1987, p. 330)

$$\sigma_{\tilde{\nu}} = \frac{1}{2N^{1/2} f(\tilde{\nu})}\,, \qquad (28)$$

where $f(\tilde{v})$ is the probability density distribution evaluated at the median point. For our sample we write $f(\tilde{v}) = \Delta N/N\Delta v$, since f should be normalized to unity. Taking $\Delta N = 0.5N^{1/2}$, we define the two-sided errors

$$\sigma_{\tilde{v}}^{+} = v(N/2 + N^{1/2}/2) - \tilde{v}\,, \tag{29a}$$

$$\sigma_{\tilde{v}}^{-} = v(N/2 - N^{1/2}/2) - \tilde{v}\,, \tag{29b}$$

for the sorted sample of v.

3. RESULTS

The results of our calculations for the individual clusters are presented in Table 3. Here we show the destruction rates for the two galactic models and the isotropic kinematics of the clusters (the anisotropic model is omitted for brevity). The Weinberg adiabatic correction is assumed throughout the table. The first two columns identify the clusters and are the same as in Table 1. The third column gives the half-mass relaxation time in years. The remaining columns present the median destruction rates per Hubble time for each cluster in the sample. The first is the evaporation rate, followed by the runs including the tidal shocks: first- and second-order disk shock, and first order disk + bulge shocks for both the galactic models. The seventh and tenth columns give the total destruction rates corresponding to our present globular clusters. The rest of this section discusses the statistical results for the sample.

3.1. *Evaporation*

We turn first to the evaporation of stars from the clusters. In other words, we perform a set of integrations in which we allow only for ordinary two-body relaxation and mass loss over the tidal boundary. Although many studies have been devoted to normal two-body relaxation, we are unaware of any complete survey of a distribution of destruction times for different cluster parameters. Figure 6 shows the evaporation time in units of the initial relaxation time versus cluster structural parameter, concentration $c = \log (R_t/R_c)$, where R_t and R_c are the tidal and core radii, respectively.

Almost all points on this figure lie along one curve. This makes it very useful for quick estimates of the evaporation time, given the initial parameters of a cluster. The least-squares fit gives

$$\frac{T_{\rm rh}}{T_{\rm ev}} = 1.290 \times 10^{-1} - 1.170 \times 10^{-1} c + 3.282 \times 10^{-2} c^2 + \frac{7.355 \times 10^{-4}}{(c - 0.55)^2}\,, \tag{30}$$

where $T_{\rm rh}$ is the half-mass relaxation time and $T_{\rm ev}$ is the total evaporation time. Our fit is shown on Figure 6 as a solid line.

This result suggests that the loosely bound clusters, with $c < 0.65$, are destroyed very fast (in units of the relaxation time). The most stable against relaxation are the clusters with $c = 1.5$–2, which survive for about $40t_{\rm rh}$. But this number decreases to $20t_{\rm rh}$ as the concentration rises beyond 2. Similar behavior has been found by Johnstone (1993; his Fig. 2).

The correlation between $T_{\rm ev}$ and $T_{\rm rh}$ could be attributed to the fact that the King models (the initial condition for our calculations) belong to a one-parameter family and so can be described by the concentration parameter only. This holds only for the dimensionless quantities, such as the ratio $T_{\rm ev}/T_{\rm rh}$. The plot of the current relaxation time, expressed in years (Fig. 7) does not show any obvious correlation with the concentration of the clusters.

3.2. *Gravitational Shocks*

Inclusion of the gravitational shocks speeds up the destruction of the clusters dramatically. Table 4 summarizes the results of our simulations when all the physical processes are acting on the clusters. The destruction rates are calculated as medians for the sample (see § 2.7). In the OC galactic model, the shocks almost double the destruction rate due to relaxation. Disk shocking (the old first-order term) has little effect for both isotropic and anisotropic kinematic models, but the shock-induced relaxation is more

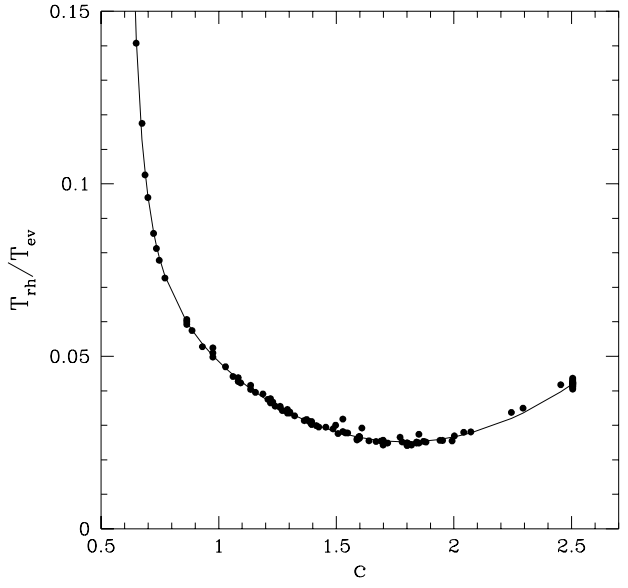

FIG. 6.—Evaporation time in units of initial relaxation time vs. cluster concentration. Dots are the results of the Fokker-Planck calculations with the observational data as input. The solid line is our fit; see eq. (30).

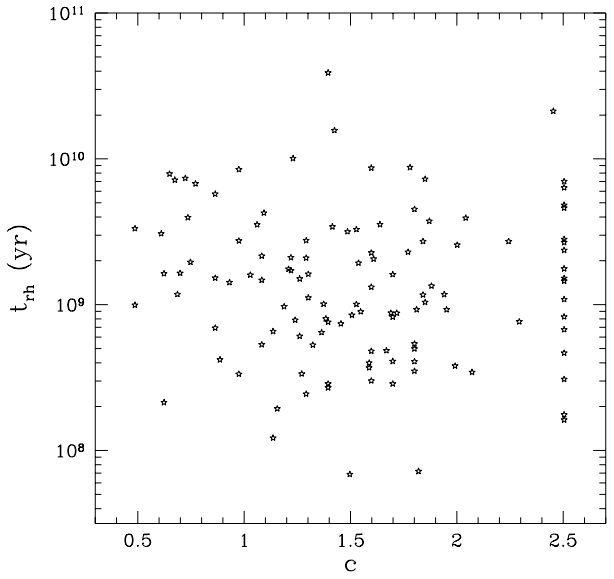

FIG. 7.—Relaxation time at the half-mass radius vs. cluster concentration for our sample of globular clusters.

TABLE 3

DESTRUCTION RATES FOR CLUSTERS IN SAMPLE[a]

ID	NAME	t_{rh} (yr)	ν_{evap}	OC ISOTROPIC			BSS ISOTROPIC		
				ν_{d1+d2}	ν_{d1+b1}	ν_{tot}	ν_{d1+d2}	ν_{d1+b1}	ν_{tot}
1	NGC 0104	3.94e+09	7.10e−02	7.84e−02	7.36e−02	7.91e−02	1.37e−01	1.11e−01	1.49e−01
2	NGC 0288	1.42e+09	3.71e−01	4.03e−01	4.47e+00	1.93e+01	8.80e−01	6.37e−01	1.10e+00
3	NGC 0362	1.18e+09	2.18e−01	2.28e−01	2.24e−01	2.33e−01	3.34e−01	2.85e−01	3.54e−01
4	NGC 1261	1.51e+09	2.33e−01	2.39e−01	2.39e−01	2.48e−01	2.74e−01	2.50e−01	2.79e−01
5	Pal 1	6.87e+07	4.37e+00	5.34e+00	1.39e+01	2.26e+01	4.47e+00	4.47e+00	4.49e+00
6	AM1	1.72e+09	2.20e−01	4.03e−01	3.80e−01	6.02e−01	2.20e−01	2.20e−01	2.20e−01
7	Eridanus	2.16e+09	2.03e−01	2.07e−01	2.04e−01	2.06e−01	2.03e−01	2.03e−01	2.03e−01
8	Pal 2	2.87e+08	1.06e+00	1.06e+00	1.09e+00	1.08e+00	1.06e+00	1.06e+00	1.06e+00
9	NGC 1851	2.72e+09	1.24e−01	1.27e−01	1.25e−01	1.27e−01	1.28e−01	1.26e−01	1.24e−01
10.....	NGC 1904	8.77e+08	2.83e−01	2.85e−01	2.84e−01	2.84e−01	3.40e−01	3.10e−01	3.54e−01
11.....	NGC 2298	3.36e+08	1.02e+00	1.02e+00	1.02e+00	1.05e+00	1.03e+00	1.02e+00	1.03e+00
12.....	NGC 2419	3.90e+10	7.97e−03	8.00e−03	7.98e−03	7.99e−03	7.97e−03	8.03e−03	8.01e−03
13.....	NGC 2808	2.30e+09	1.16e−01	1.10e−01	1.10e−01	1.11e−01	1.50e−01	1.32e−01	1.61e−01
14.....	Pal 3	8.46e+09	5.88e−02	5.88e−02	5.88e−02	5.88e−02	5.88e−02	5.88e−02	5.88e−02
15.....	NGC 3201	1.62e+09	2.07e−01	2.63e−01	2.28e−01	2.69e−01	3.30e−01	2.65e−01	3.45e−01
16.....	Pal 4	7.38e+09	1.16e−01	1.16e−01	1.16e−01	1.16e−01	1.16e−01	1.16e−01	1.16e−01
17.....	NGC 4147	5.00e+08	4.83e−01	4.84e−01	4.84e−01	4.84e−01	4.83e−01	4.83e−01	4.83e−01
18.....	NGC 4372	2.76e+09	1.24e−01	1.48e−01	1.36e−01	1.58e−01	4.59e−01	3.04e−01	4.74e−01
19.....	Rup 106	1.64e+09	5.03e+00	7.88e+00	6.00e+00	7.97e+00	5.11e+00	5.05e+00	5.13e+00
20.....	NGC 4590	3.56e+09	7.17e−02	1.08e−01	8.16e−02	9.82e−02	8.12e−02	7.55e−02	8.22e−02
21.....	NGC 4833	7.86e+08	4.52e−01	4.83e−01	5.91e−01	7.65e−01	1.60e+00	2.40e+00	4.36e+00
22.....	NGC 5024	8.74e+09	2.88e−02	2.84e−02	2.88e−02	2.88e−02	3.03e−02	2.96e−02	3.07e−02
23.....	NGC 5053	6.76e+09	1.07e−01	2.46e+00	4.81e+00	1.39e+01	1.36e+00	2.40e−01	1.62e+00
24.....	NGC 5139	1.01e+10	3.65e−02	6.58e−02	1.01e−01	1.60e−01	1.49e−01	1.92e−01	3.43e−01
25.....	NGC 5272	7.28e+09	3.41e−02	4.01e−02	3.66e−02	3.98e−02	5.19e−02	4.29e−02	5.42e−02
26.....	NGC 5286	7.42e+08	3.97e−01	4.00e−01	3.96e−01	4.01e−01	4.57e−01	1.07e+00	1.57e+00
27.....	NGC 5466	1.57e+10	1.88e−02	1.02e+00	4.69e−01	3.01e+00	1.66e+00	4.30e−01	2.73e+00
28.....	NGC 5634	2.27e+09	1.18e−01	1.18e−01	1.17e−01	1.19e−01	1.15e−01	1.18e−01	1.15e−01
29.....	NGC 5694	1.17e+09	2.13e−01	2.11e−01	2.17e−01	2.13e−01	2.10e−01	2.10e−01	2.10e−01
30.....	IC 4499	4.26e+09	9.93e−02	1.07e−01	1.02e−01	1.11e−01	4.57e−01	2.34e−01	4.76e−01
31.....	NGC 5824	2.13e+10	1.96e−02	2.08e−02	2.02e−02	2.10e−02	2.71e−02	2.41e−02	3.06e−02
32.....	Pal 5	7.17e+09	1.64e−01	2.37e+00	3.79e+00	9.62e+00	1.74e−01	1.66e−01	2.16e−01
33.....	NGC 5897	3.96e+09	2.05e−01	1.49e+00	6.55e+00	1.85e+01	3.71e+01	1.63e+02	4.18e+02
34.....	NGC 5904	3.75e+09	6.76e−02	8.61e−02	8.57e−02	1.08e−01	4.06e−01	1.11e+00	1.76e+00
35.....	NGC 5927	1.32e+09	1.98e−01	2.23e−01	2.14e−01	2.43e−01	3.57e−01	2.71e−01	3.49e−01
36.....	NGC 5946	6.36e+09	6.80e−02	1.73e−01	2.17e−01	3.43e−01	2.32e−01	1.46e−01	2.38e−01
37.....	NGC 5986	1.76e+09	2.13e−01	2.20e−01	9.37e−01	1.74e+00	5.42e−01	1.81e+00	9.70e+00
38.....	Pal 14	7.90e+09	1.78e−01	1.78e−01	1.83e−01	1.96e−01	3.97e+00	9.41e+00	2.05e+01
39.....	NGC 6093	9.26e+08	2.77e−01	2.84e−01	2.88e+00	4.20e+00	7.68e−01	1.35e+00	1.86e+00
40.....	NGC 6101	1.96e+09	3.97e−01	4.05e−01	4.00e−01	4.05e−01	9.38e+00	1.32e+01	3.76e+01
41.....	NGC 6121	3.70e+08	7.05e−01	7.16e−01	7.54e−01	8.30e−01	7.38e−01	7.37e−01	7.52e−01
42.....	NGC 6144	2.10e+09	1.65e−01	3.26e−01	4.78e−01	7.21e−01	1.71e+00	9.30e−01	2.00e+00
43.....	NGC 6139	5.40e+08	4.53e−01	4.56e−01	4.55e−01	4.61e−01	7.13e−01	2.16e+00	3.07e+00
44.....	NGC 6171	8.48e+08	3.26e−01	3.57e−01	3.40e−01	3.77e−01	5.59e−01	4.22e−01	5.48e−01
45.....	NGC 6205	3.17e+09	9.13e−02	1.23e−01	1.15e−01	1.47e−01	1.01e−01	9.55e−02	1.02e−01
46.....	NGC 6218	1.01e+09	3.13e−01	3.16e−01	3.87e−01	4.68e−01	3.78e−01	3.39e−01	3.84e−01
47.....	NGC 6229	2.06e+09	1.41e−01	1.28e−01	1.27e−01	1.28e−01	1.27e−01	1.28e−01	1.31e−01
48.....	NGC 6235	5.30e+08	6.18e−01	6.20e−01	6.78e+00	3.26e+01	9.06e−01	7.99e−01	1.02e+00
49.....	NGC 6254	7.60e+08	4.01e−01	4.33e−01	4.51e−01	5.03e−01	4.22e−01	4.08e−01	4.23e−01
50.....	NGC 6256	4.67e+08	8.68e−01	8.95e−01	9.72e−01	1.08e+00	1.76e+00	1.29e+00	1.78e+00
51.....	Pal 15	3.33e+09	3.80e+02	3.80e+02	3.80e+02	3.80e+02	3.81e+02	3.81e+02	3.83e+02
52.....	NGC 6266	4.09e+08	6.27e−01	6.28e−01	6.33e−01	6.44e−01	6.26e−01	6.31e−01	6.38e−01
53.....	NGC 6273	3.29e+09	9.68e−02	9.24e−02	1.02e−01	1.20e−01	2.89e−01	4.72e+00	2.46e+01
54.....	NGC 6284	4.82e+09	8.68e−02	4.69e−01	3.79e−01	5.98e−01	2.26e+00	3.11e+00	5.34e+00
55.....	NGC 6287	3.01e+08	8.88e−01	8.70e−01	1.52e+00	2.09e+00	9.78e−01	9.62e−01	1.13e+00
56.....	NGC 6293	1.45e+09	2.88e−01	3.02e−01	6.88e+00	9.66e+00	1.47e+00	6.21e+00	9.05e+00
57.....	NGC 6304	4.08e+08	5.94e−01	6.08e−01	2.91e+00	4.37e+00	6.60e−01	6.22e−01	6.74e−01
58.....	NGC 6316	8.97e+08	3.10e−01	3.06e−01	6.71e−01	9.61e−01	3.31e−01	3.09e−01	3.13e−01
59.....	NGC 6325	3.08e+08	1.33e+00	1.35e+00	2.52e+00	3.54e+00	1.66e+00	1.45e+00	1.67e+00
60.....	NGC 6341	9.27e+08	2.65e−01	2.68e−01	2.64e−01	2.66e−01	3.60e−01	3.25e−01	4.01e−01
61.....	NGC 6333	6.57e+08	6.15e−01	6.18e−01	6.19e−01	6.26e−01	7.24e−01	1.82e+00	3.11e+00
62.....	NGC 6342	2.36e+09	1.80e−01	3.23e−01	3.09e−01	4.53e−01	1.66e+00	3.55e+00	5.27e+00
63.....	NGC 6356	1.94e+09	1.44e−01	1.43e−01	1.44e−01	1.43e−01	1.82e−01	1.59e−01	1.83e−01
64.....	NGC 6355	1.52e+09	2.79e−01	2.96e−01	3.78e−01	4.89e−01	9.20e−01	1.59e+00	2.47e+00
65.....	NGC 6352	5.33e+08	8.02e−01	8.14e−01	8.06e−01	8.14e−01	1.04e+00	8.93e−01	1.05e+00
66.....	NGC 6366	4.20e+08	1.37e+00	1.41e+00	1.45e+00	1.63e+00	3.25e+00	3.13e+00	8.64e+00
67.....	NGC 6362	1.48e+09	2.90e−01	4.26e−01	3.64e−01	4.78e−01	7.29e−01	4.60e−01	7.35e−01
68.....	NGC 6388	8.25e+08	3.08e−01	3.07e−01	3.08e−01	3.16e−01	3.22e−01	3.18e−01	3.53e−01
69.....	NGC 6402	8.68e+09	3.08e−02	7.99e−02	4.72e+00	2.06e+01	2.65e−01	2.17e−01	3.32e−01
70.....	NGC 6401	8.78e+08	2.89e−01	2.90e−01	7.69e−01	1.09e+00	2.97e−01	3.02e−01	3.00e−01
71.....	NGC 6397	1.76e+08	2.35e+00	2.36e+00	2.36e+00	2.42e+00	2.43e+00	2.37e+00	2.48e+00

TABLE 3—*Continued*

ID	NAME	t_{rh} (yr)	v_{evap}	OC ISOTROPIC			BSS ISOTROPIC		
				v_{d1+d2}	v_{d1+b1}	v_{tot}	v_{d1+d2}	v_{d1+b1}	v_{tot}
72	NGC 6426	1.61e+09	1.51e−01	2.54e−01	2.25e−01	3.14e−01	1.77e−01	1.63e−01	1.86e−01
73	NGC 6440	2.87e+08	8.77e−01	8.78e−01	8.78e−01	8.89e−01	9.01e−01	8.98e−01	9.05e−01
74	NGC 6441	1.04e+09	2.64e−01	2.42e−01	3.39e−01	4.28e−01	2.74e−01	2.57e−01	2.86e−01
75	NGC 6453	2.81e+09	1.51e−01	8.28e−01	8.88e−01	1.38e+00	3.51e+00	2.40e+00	3.66e+00
76	NGC 6496	2.14e+08	3.85e+01	3.86e+01	1.69e+02	3.36e+02	5.97e+01	1.55e+02	3.05e+02
77	NGC 6517	7.21e+07	3.37e+00	3.37e+00	3.50e+00	3.46e+00	3.46e+00	3.37e+00	3.40e+00
78	NGC 6522	8.28e+08	4.98e−01	8.31e−01	3.24e+00	5.04e+00	5.23e+00	6.08e+00	9.18e+00
79	NGC 6535	2.45e+08	1.37e+00	1.40e+00	1.54e+00	1.79e+00	1.81e+00	1.66e+00	1.97e+00
80	NGC 6528	7.65e+08	4.57e−01	6.90e−01	1.99e+00	3.00e+00	2.65e+00	2.58e+00	3.89e+00
81	NGC 6539	4.81e+08	5.47e−01	5.44e−01	5.37e−01	5.49e−01	5.83e−01	5.54e−01	5.92e−01
82	NGC 6544	1.62e+08	2.55e+00	2.55e+00	2.55e+00	2.55e+00	2.55e+00	2.55e+00	2.55e+00
83	NGC 6541	2.57e+09	1.05e−01	1.80e−01	1.74e−01	2.42e−01	5.31e−01	4.50e−01	6.42e−01
84	NGC 6553	1.94e+08	2.04e+00	2.04e+00	2.04e+00	2.10e+00	2.05e+00	2.04e+00	2.05e+00
85	NGC 6558	1.09e+09	3.85e−01	3.93e−01	1.52e+00	2.41e+00	2.56e+00	3.74e+01	5.57e+01
86	NGC 6569	6.09e+08	5.82e−01	5.80e−01	1.35e+00	2.01e+00	9.62e−01	5.96e+00	3.05e+01
87	NGC 6584	9.72e+08	4.02e−01	4.03e−01	4.41e−01	5.18e−01	6.82e−01	6.28e−01	8.54e−01
88	NGC 6624	2.68e+09	1.58e−01	1.62e−01	1.32e+00	1.83e+00	1.86e+00	2.79e+00	3.94e+00
89	NGC 6626	4.84e+08	5.22e−01	5.28e−01	5.29e−01	5.46e−01	6.96e−01	1.09e+00	1.49e+00
90	NGC 6638	2.70e+08	1.12e+00	1.13e+00	8.22e+00	1.41e+01	1.70e+00	3.07e+00	4.39e+00
91	NGC 6637	8.03e+08	3.88e−01	3.91e−01	1.21e+00	1.81e+00	5.37e−01	4.63e−01	5.45e−01
92	NGC 6642	3.81e+08	6.69e−01	7.03e−01	1.38e+00	1.90e+00	1.88e+00	4.03e+00	5.56e+00
93	NGC 6652	3.51e+08	7.08e−01	6.95e−01	7.08e−01	7.28e−01	6.96e−01	6.94e−01	6.95e−01
94	NGC 6656	1.12e+09	3.03e−01	3.11e−01	3.06e−01	3.15e−01	3.24e−01	3.09e−01	3.21e−01
95	Pal8	1.18e+09	8.70e−01	8.72e−01	8.71e−01	8.72e−01	8.70e−01	8.70e−01	8.70e−01
96	NGC 6681	6.75e+08	6.34e−01	6.26e−01	6.51e−01	7.09e−01	8.55e−01	1.06e+00	1.48e+00
97	NGC 6712	6.94e+08	8.54e−01	8.57e−01	1.03e+00	1.35e+00	1.16e+00	7.46e+00	3.59e+01
98	NGC 6715	2.72e+09	9.24e−02	9.41e−02	9.41e−02	9.56e−02	1.83e−01	2.90e−01	4.03e−01
99	NGC 6717	3.44e+08	8.15e−01	7.99e−01	6.04e+00	8.97e+00	1.80e+00	4.30e+00	6.13e+00
100.....	NGC 6723	1.60e+09	2.93e−01	2.97e−01	2.96e−01	3.21e−01	5.04e−01	4.09e−01	5.77e−01
101.....	NGC 6752	4.61e+09	9.19e−02	2.40e−01	1.60e−01	2.44e−01	3.08e−01	2.04e−01	3.23e−01
102.....	NGC 6760	3.99e+08	6.45e−01	6.87e−01	6.69e−01	7.16e−01	9.49e−01	8.86e−01	1.11e+00
103.....	Terzan 7	3.55e+09	1.24e−01	1.26e−01	1.29e−01	1.28e−01	1.28e−01	1.25e−01	1.25e−01
104.....	NGC 6779	6.46e+08	4.86e−01	4.90e−01	4.88e−01	5.01e−01	5.21e−01	5.12e−01	5.24e−01
105.....	Arp 2	5.75e+09	1.04e−01	1.21e−01	1.22e−01	1.61e−01	3.59e+01	1.94e+01	6.02e+01
106.....	NGC 6809	1.64e+09	5.84e−01	6.03e−01	6.42e−01	7.52e−01	6.67e−01	6.06e−01	6.83e−01
107.....	Terzan 8	9.94e+08	1.27e+03	1.28e+03	1.28e+03	1.28e+03	1.28e+03	1.28e+03	1.28e+03
108.....	Pal 11	3.07e+09	7.62e+00	1.21e+01	9.16e+00	1.21e+01	1.36e+01	9.85e+00	1.38e+01
109.....	NGC 6838	1.22e+08	3.40e+00	3.33e+00	3.41e+00	3.34e+00	3.34e+00	3.35e+00	3.34e+00
110.....	NGC 6864	1.35e+09	1.87e−01	1.91e−01	1.88e−01	1.92e−01	1.91e−01	1.88e−01	1.89e−01
111.....	NGC 6934	1.01e+09	2.80e−01	2.74e−01	2.74e−01	2.75e−01	2.85e−01	2.77e−01	2.89e−01
112.....	NGC 6981	2.11e+09	1.73e−01	1.79e−01	1.74e−01	1.76e−01	1.83e−01	1.74e−01	1.76e−01
113.....	NGC 7006	3.43e+09	8.72e−02	8.96e−02	8.83e−02	9.02e−02	8.72e−02	8.73e−02	8.72e−02
114.....	NGC 7078	7.01e+09	6.23e−02	1.18e−01	1.35e−01	2.03e−01	2.02e−01	1.38e−01	2.17e−01
115.....	NGC 7089	4.52e+09	5.51e−02	7.59e−02	6.74e−02	8.13e−02	5.85e−02	5.66e−02	5.76e−02
116.....	NGC 7099	1.77e+09	2.38e−01	2.70e−01	2.55e−01	2.88e−01	4.65e−01	4.04e−01	5.65e−01
117.....	Pal 12	1.52e+09	3.98e−01	4.12e−01	4.12e−01	4.15e−01	3.79e+00	1.06e+00	7.12e+00
118.....	Pal 13	3.34e+08	1.57e+00	1.57e+00	1.57e+00	1.57e+00	1.57e+00	1.57e+00	1.57e+00
119.....	NGC 7492	2.75e+09	1.85e−01	2.24e−01	2.28e−01	3.16e−01	4.72e+00	3.79e+00	1.44e+01

NOTE.—The rates including the tidal shocks are v_{d1+d2}, first- and second-order disk shock; v_{d1+b1}, first-order disk and bulge shocks; v_{tot}, total destruction rate (first- and second-order disk + bulge shocks). The two groups of columns correspond to the results for the OC and BSS galactic models. In both cases the isotropic kinematic model is assumed, appropriate for the present clusters. The Weinberg form of the adiabatic correction is used (see text for more detail).

[a] Destruction rates v in units of inverse Hubble time.

pronounced (0.09 in the median rate gain versus 0.017 in the former case). The case with the Spitzer correction is enhanced in the shock relaxation and bulge shocks because of the overimpulse increase of the adiabatic corrections (§ 2.5.2). The bulge shock is much stronger, and in the isotropic model, it completely dominates over the disk shock. For the anisotropic model, the destruction associated with the bulge shock is reduced. Total destruction rate for the OC model is in the range 0.45–0.58.

In the BSS galactic model, the disk is stronger, and there is a nuclear component that dominates the tidal shock over large range of radii (cf. Fig. 4). Therefore, the destruction rates are significantly increased by the shocks: they range from 0.63 to 0.86.

Next, we investigate the dependence of the destruction rates on the currently observed cluster positions. Figure 8 shows the destruction rates associated with the several combinations of the physical mechanisms (§ 2.7) versus galactocentric radius, for the OC galactic model and isotropic kinematic model of the clusters (§ 2.3). We use here calculations with the Weinberg adiabatic correction. The left top panel, corresponding to two-body relaxation, is largely determined by the selection of our sample, since relaxation is an internal process. However, the steady increase in the rate with the decreasing distance to the galactic center is most likely explained by the growing tidal field that imposes tidal cutoff and therefore removes stars from cluster faster. Going from the left top panel to the middle bottom panel,

TABLE 4

MEDIAN DESTRUCTION RATES

DESTRUCTION PROCESS	ISOTROPIC			ANISOTROPIC	
	Spitzer	Weinberg	No Correction	Spitzer	Weinberg
Ostriker & Caldwell Model					
Evaporation	$0.290^{+0.020}_{-0.013}$	$0.290^{+0.020}_{-0.013}$	$0.290^{+0.020}_{-0.013}$	$0.290^{+0.020}_{-0.013}$	$0.290^{+0.020}_{-0.013}$
+ Disk 1st	$0.307^{+0.073}_{-0.017}$	$0.311^{+0.069}_{-0.026}$	$0.312^{+0.069}_{-0.021}$	$0.307^{+0.073}_{-0.018}$	$0.309^{+0.065}_{-0.017}$
+ Disk	$0.397^{+0.021}_{-0.086}$	$0.391^{+0.012}_{-0.080}$	$0.394^{+0.011}_{-0.049}$	$0.393^{+0.021}_{-0.074}$	$0.365^{+0.033}_{-0.049}$
+ Disk 1st + Bulge 1st	$0.467^{+0.073}_{-0.058}$	$0.455^{+0.074}_{-0.059}$	$0.601^{+0.096}_{-0.091}$	$0.398^{+0.088}_{-0.085}$	$0.397^{+0.075}_{-0.077}$
+ Disk + Bulge	$0.583^{+0.133}_{-0.053}$	$0.518^{+0.108}_{-0.039}$	$0.905^{+0.048}_{-0.183}$	$0.490^{+0.138}_{-0.091}$	$0.453^{+0.116}_{-0.056}$
Bahcall, Schmidt, & Soneira Model					
Evaporation	$0.290^{+0.020}_{-0.013}$	$0.290^{+0.020}_{-0.013}$	$0.290^{+0.020}_{-0.013}$	$0.290^{+0.020}_{-0.013}$	$0.290^{+0.020}_{-0.013}$
+ Disk 1st	$0.495^{+0.053}_{-0.088}$	$0.498^{+0.081}_{-0.075}$	$0.502^{+0.118}_{-0.027}$	$0.395^{+0.059}_{-0.057}$	$0.395^{+0.066}_{-0.049}$
+ Disk	$0.654^{+0.077}_{-0.101}$	$0.660^{+0.053}_{-0.124}$	$0.818^{+0.072}_{-0.159}$	$0.511^{+0.117}_{-0.045}$	$0.493^{+0.054}_{-0.058}$
+ Disk 1st + Bulge 1st	$0.627^{+0.164}_{-0.130}$	$0.628^{+0.171}_{-0.145}$	$1.026^{+0.383}_{-0.233}$	$0.520^{+0.061}_{-0.054}$	$0.480^{+0.057}_{-0.069}$
+ Disk + Bulge	$0.863^{+0.163}_{-0.181}$	$0.752^{+0.276}_{-0.110}$	$1.786^{+0.747}_{-0.699}$	$0.712^{+0.103}_{-0.061}$	$0.633^{+0.072}_{-0.053}$

NOTE.—Rates are in fraction of sample per Hubble time (10^{10} yr). Total number of clusters in sample: 119.

we include more and more tidal shock processes. The disk in the OC model is relatively weak and does not change the distribution noticeably. Bulge shocks, on the other hand, enhance the destruction in the center considerably. Relaxation induced by the bulge shock is comparable to the first order effect. For clusters within 2 kpc of the center of the Galaxy, tidal shock relaxation dominates ordinary two-body relaxation in determining the cluster evolution. For such clusters, core collapse occurs much faster and overall evolution proceeds on the shock timescale when it is shorter than the relaxation time. During the cluster contraction, the relative importance of the tidal shock relaxation to ordinary two-body relaxation decreases, and the final stage of core collapse is described by the self-similar solutions of Hénon (1961). After core collapse, the cluster is still so highly concentrated that the density profile is close to an isothermal sphere. Slow expansion along with the tidal stripping of stars leads to final dissolution of the cluster.

A similar plot for the anisotropic kinematic model is given in Figure 9. Figures 10 and 11 show the distribution for the BSS galactic model and the isotropic and anisotropic kinematics, respectively.

To emphasize the relative importance of each of the destruction mechanisms, we define the *differential* rates by subtracting the destruction rates obtained without that process from the run including the process. Namely, first-order disk shock ("disk 1") is "evaporation + disk 1" − "evaporation"; second-order disk shock relaxation term ("disk 2") is "evaporation + disk" − "evaporation + disk 1"; first-order bulge shock ("bulge 1") is "evaporation + disk 1 + bulge 1" − "evaporation + disk 1"; and the bulge relaxation is "evaporation + disk + bulge" − "evaporation + disk" − "bulge 1." Differential rates for the two galactic and kinematic models are presented in Figures 12, 13, 14, and 15.

We should, however, be cautious using these differential results, since all those mechanisms act together and the final result is not a direct sum of the single processes. For example, relaxation is enhanced by the tidal shock relaxation, and core collapse occurs faster (in some cases clusters collapsed even when the ordinary relaxation was not enough to drive the contraction). For the above reasons, these figures must be considered indicative but not exact.

We present the histograms of the distributions of the destruction rates in Figures 16, 17, 18, and 19. Arrows at the top show median of the distribution.

The main difference between the OC and BSS galactic models is the stronger BSS disk. Outside the solar radius, the effect of tidal shocks is profoundly more important in the BSS model than in the OC. Toward the center, both models predict a sharp rise of the destruction rate with a little stronger imprint of the OC bulge. In the competition between themselves, the bulge shocks dominate in the central parts of the Galaxy, and the disk shocks, in the outer. In the BSS model, the transition occurs at about 2 kpc, whereas the weaker disk of the OC model overtakes the bulge only outside 4 kpc.

3.3. *Consistency Test for the Initial Conditions*[3]

In our choice of initial conditions, we made one assumption, different from that used by AHO, which should be examined. To complement the limited observed orbital parameters of the globular clusters, we have drawn the two random transverse velocity components (§ 2.3). These initial conditions define the cluster orbits and, through them, the median perigalactic points. Some of the orbits might produce perigalactica so small as to lead to tidal radii much smaller than the observed tidal radii of the clusters. These orbits should have been rejected from consideration. Using the simple theoretical relation (eq. [26]), we obtain an estimate of the tidal radius that can be compared with the observed values. For the core-collapsed clusters, the observational determination of the R_t is very difficult and indefinite, and less weight should be assigned to them in the comparison with the calculations.

The orbits we used for the Fokker-Planck simulations reported above impose tidal radii that have substantial deviations from the observed R_t in both positive and negative directions, as shown in Figure 20. Still, there is a clear trend toward the smaller radii. The reason for this asym-

[3] This subsection has been added in response to the comments of the referee.

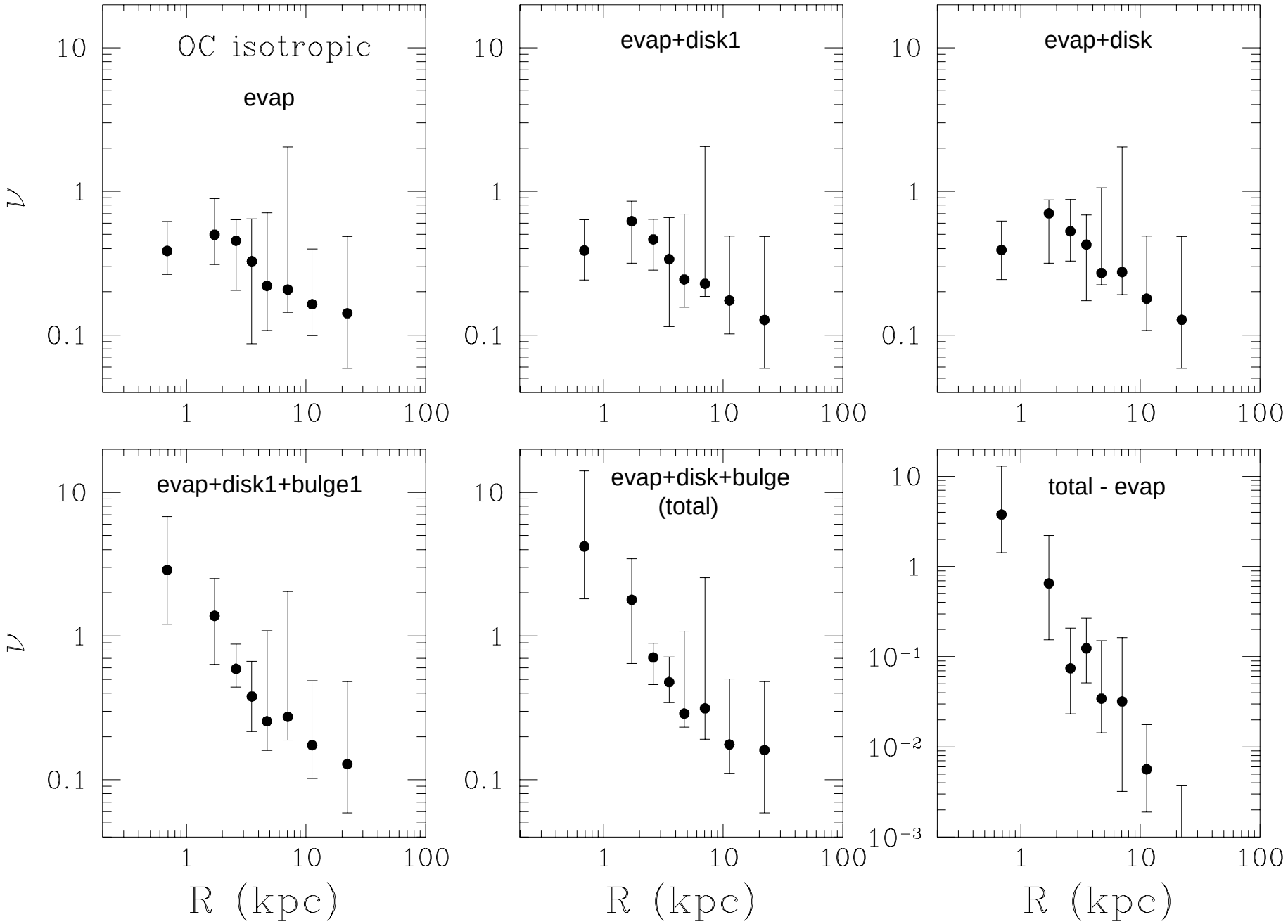

FIG. 8.—Mean probability per Hubble time for cluster destruction due to evaporation, and the evaporation plus gravitational shocks: disk shock without relaxation, disk shock including relaxation term, disk + bulge shocks without relaxation, and disk + bulge shock including relaxation, as a function of present-day galactocentric distance. The error bars indicate the interquartile range of the distribution. Weinberg adiabatic corrections are used. Galactic model is OC, and kinematic model is isotropic.

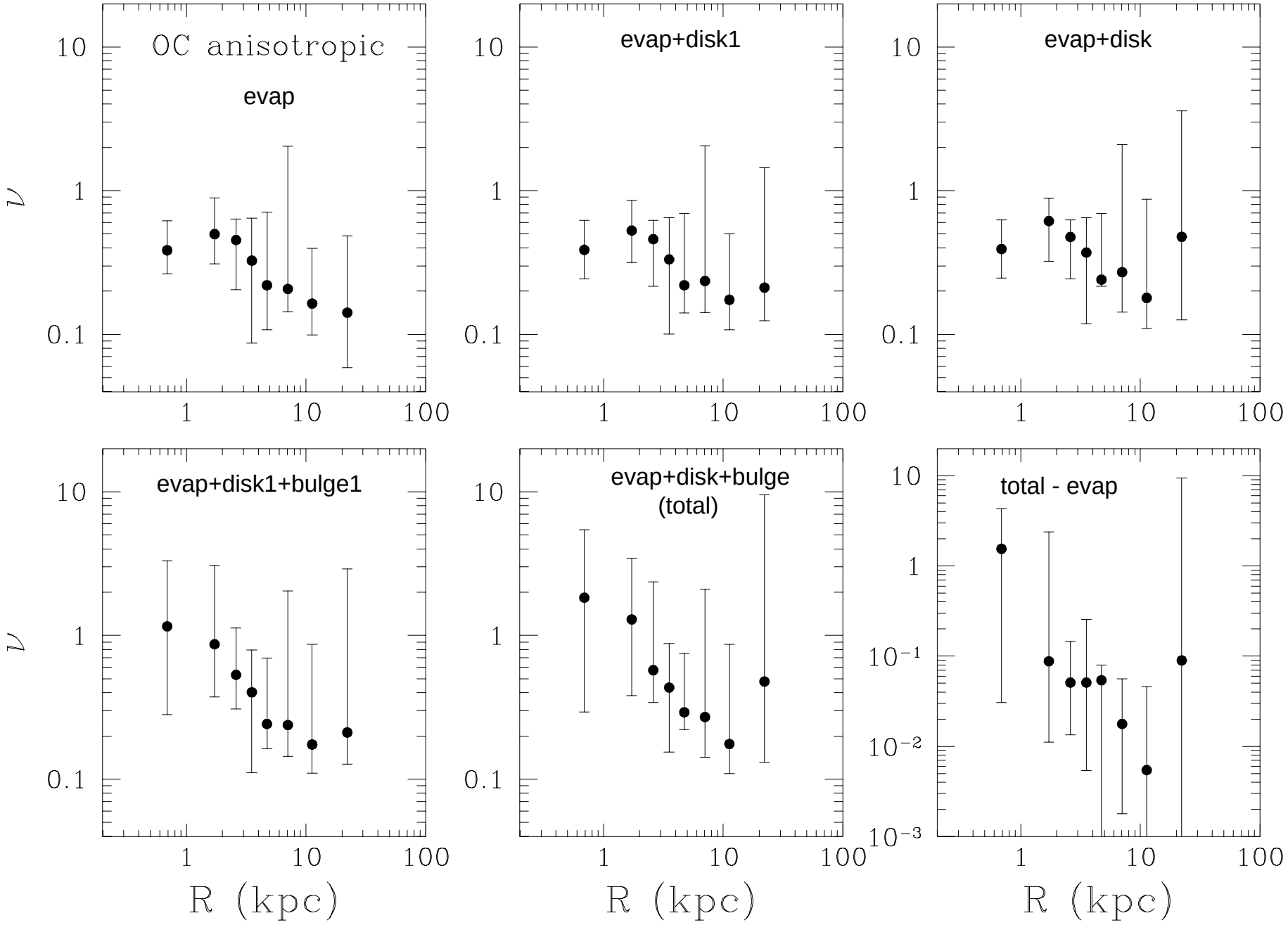

FIG. 9.—Same as Fig. 8, but for the anisotropic kinematic model

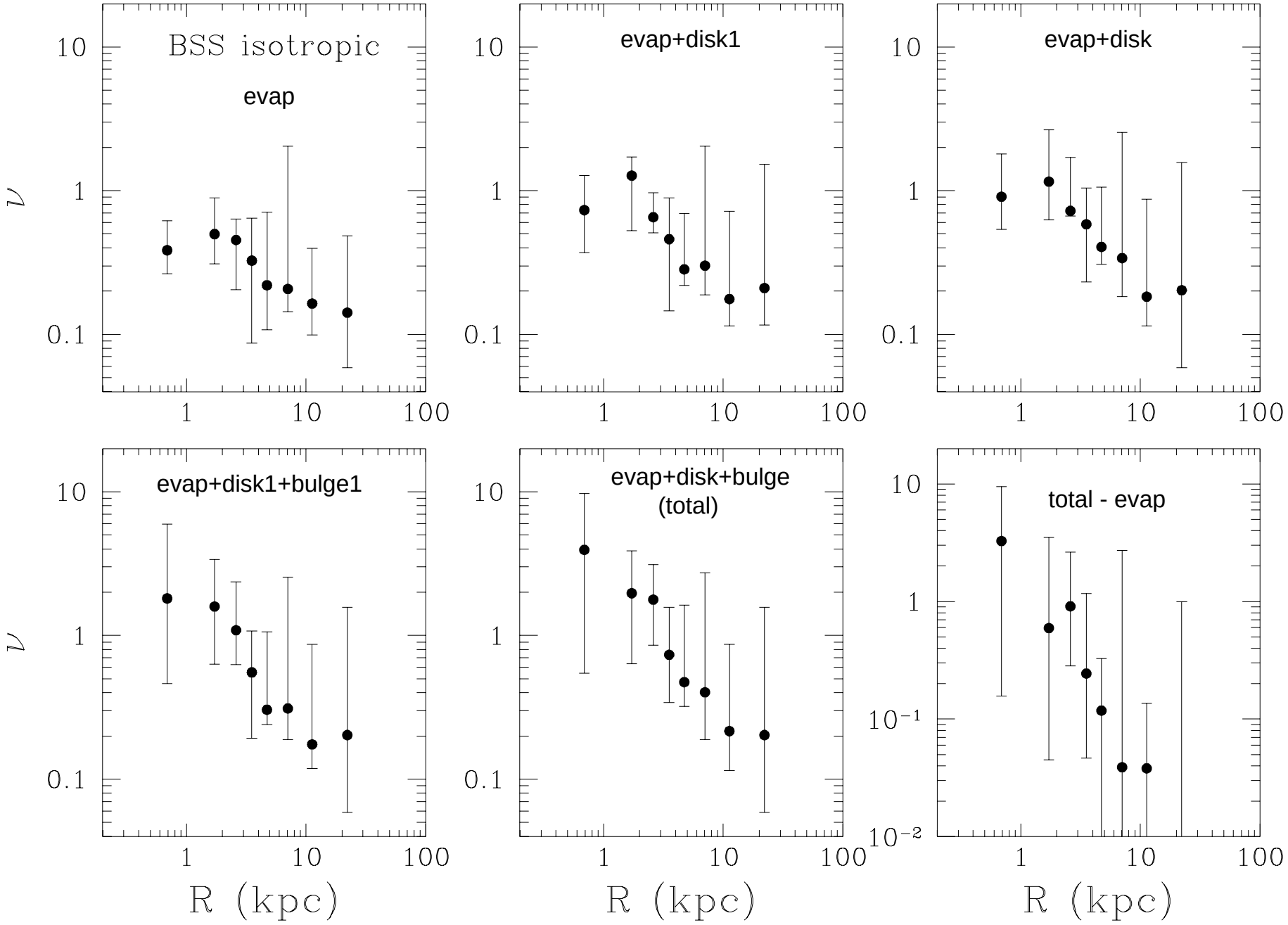

FIG. 10.—Same as Fig. 8, but for the BSS galactic model

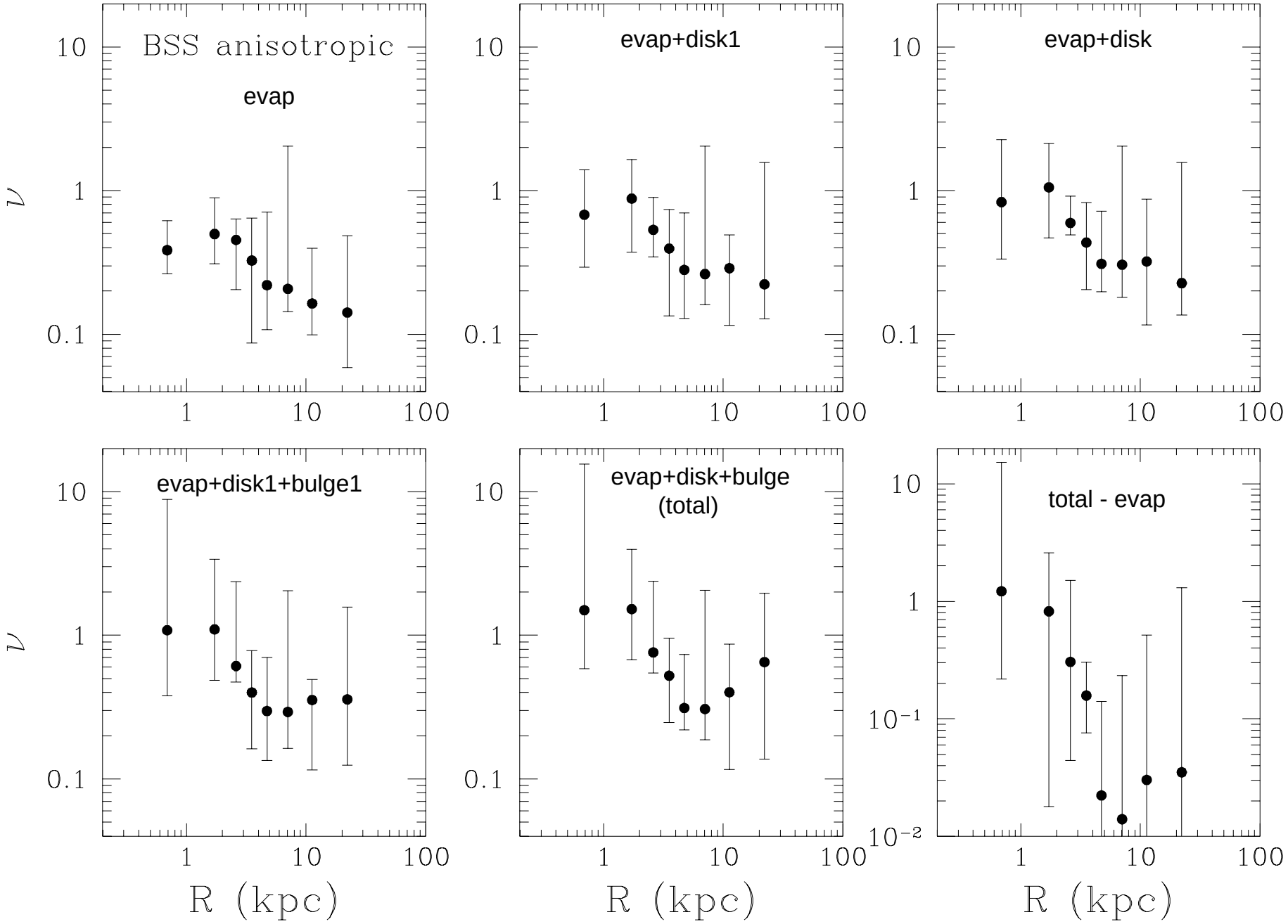

FIG. 11.—Same as Fig. 9, but for the BSS galactic model

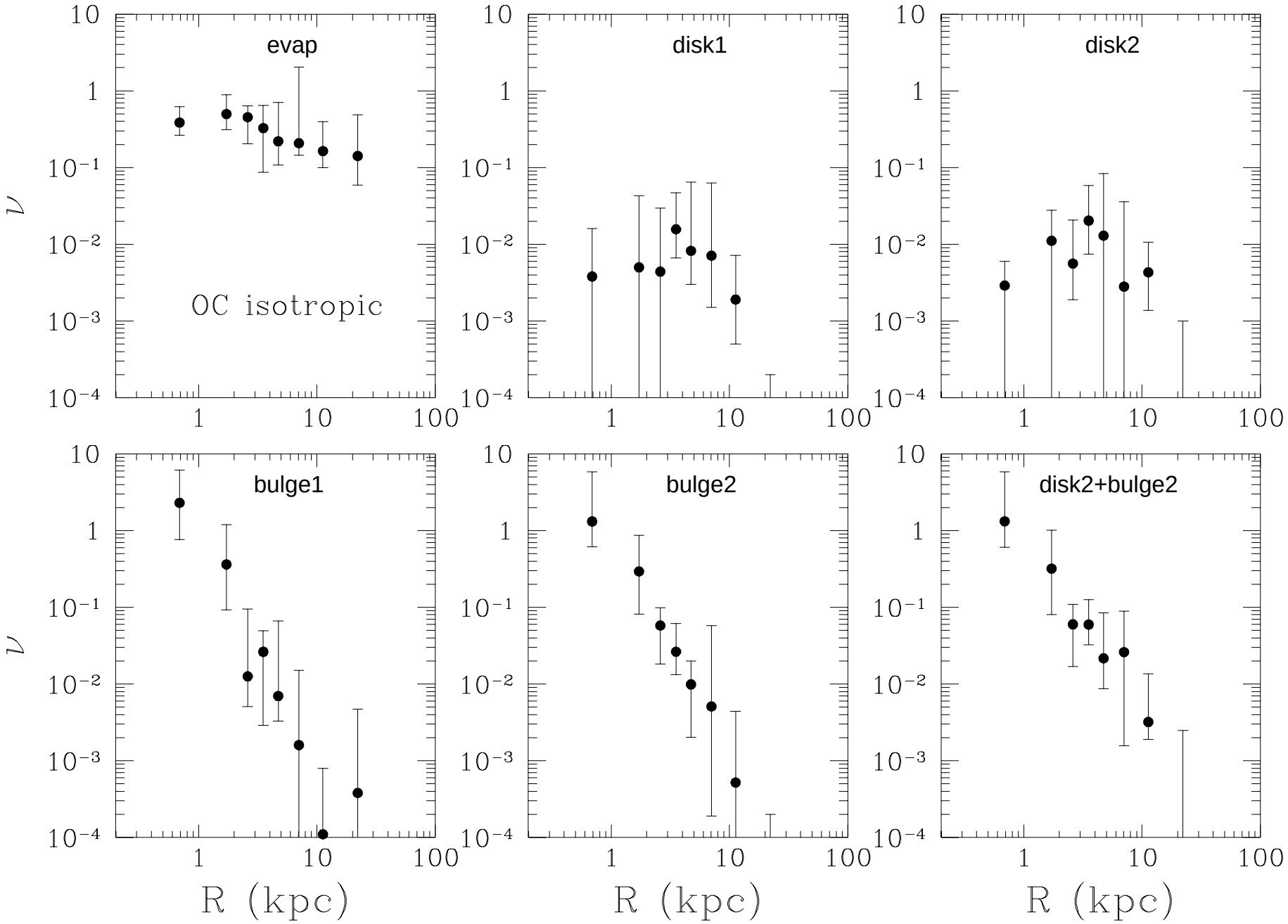

FIG. 12.—Differential destruction rate for different processes: evaporation, disk shock with and without induced relaxation ("disk 1" and "disk", respectively), and bulge shock with and without relaxation term ("bulge 1" and "bulge"). See text for the definition of the differential rate. The error bars indicate the interquartile range of the distribution. Weinberg adiabatic corrections are used. Galactic model is OC, and kinematic model is isotropic.

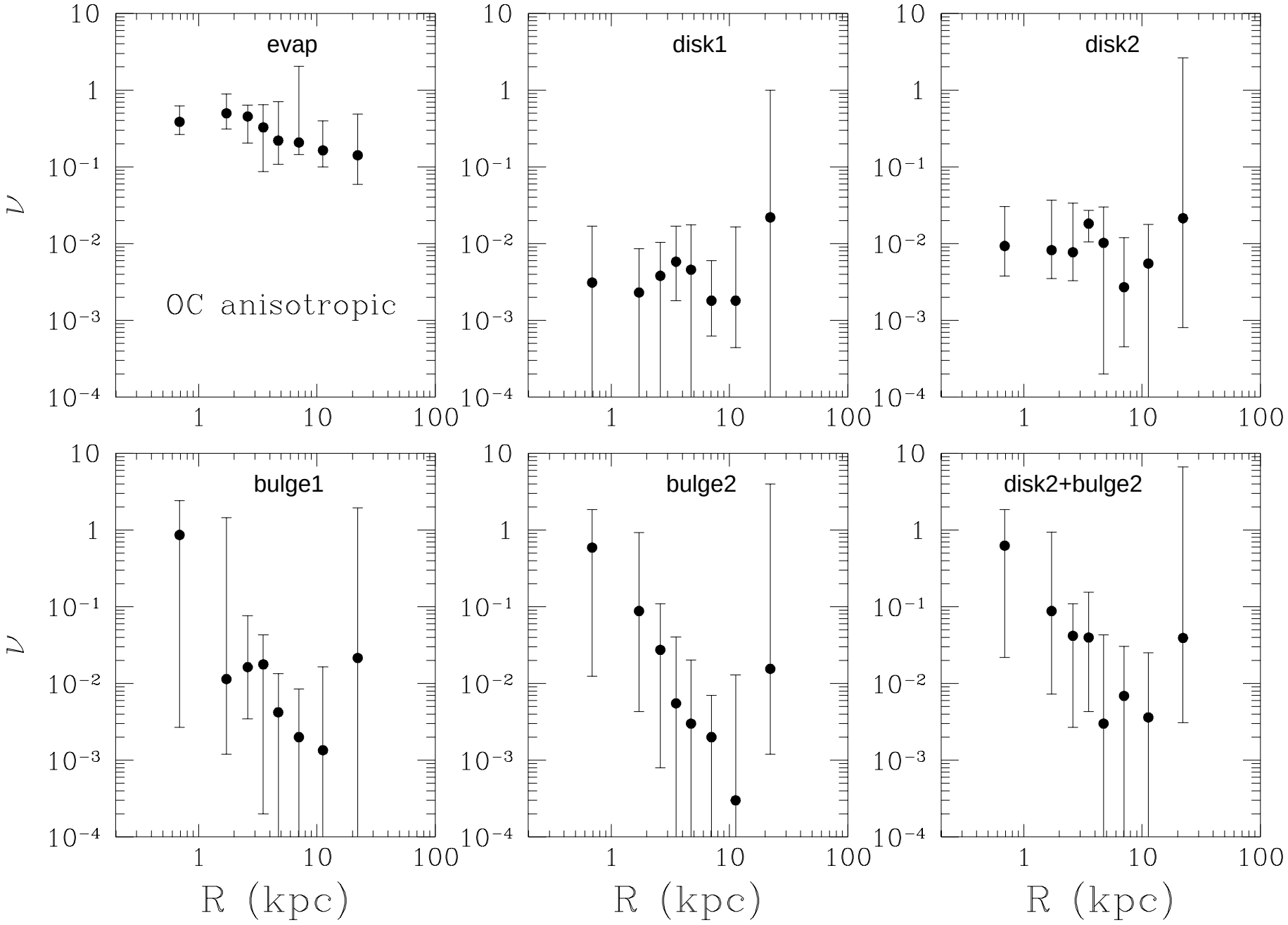

FIG. 13.—Same as Fig. 12, but for the anisotropic kinematic model

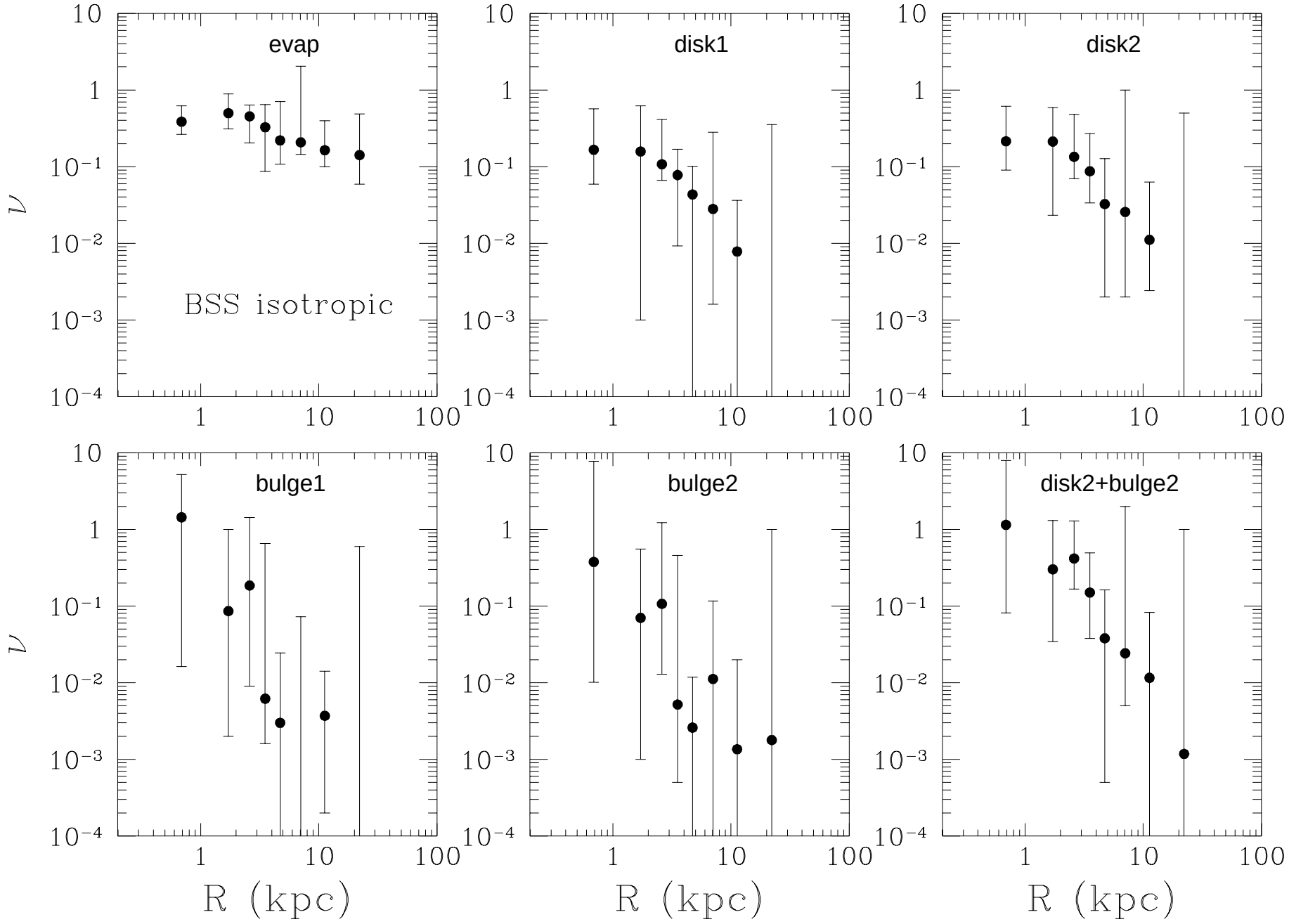

FIG. 14.—Same as Fig. 12, but for the BSS galactic model

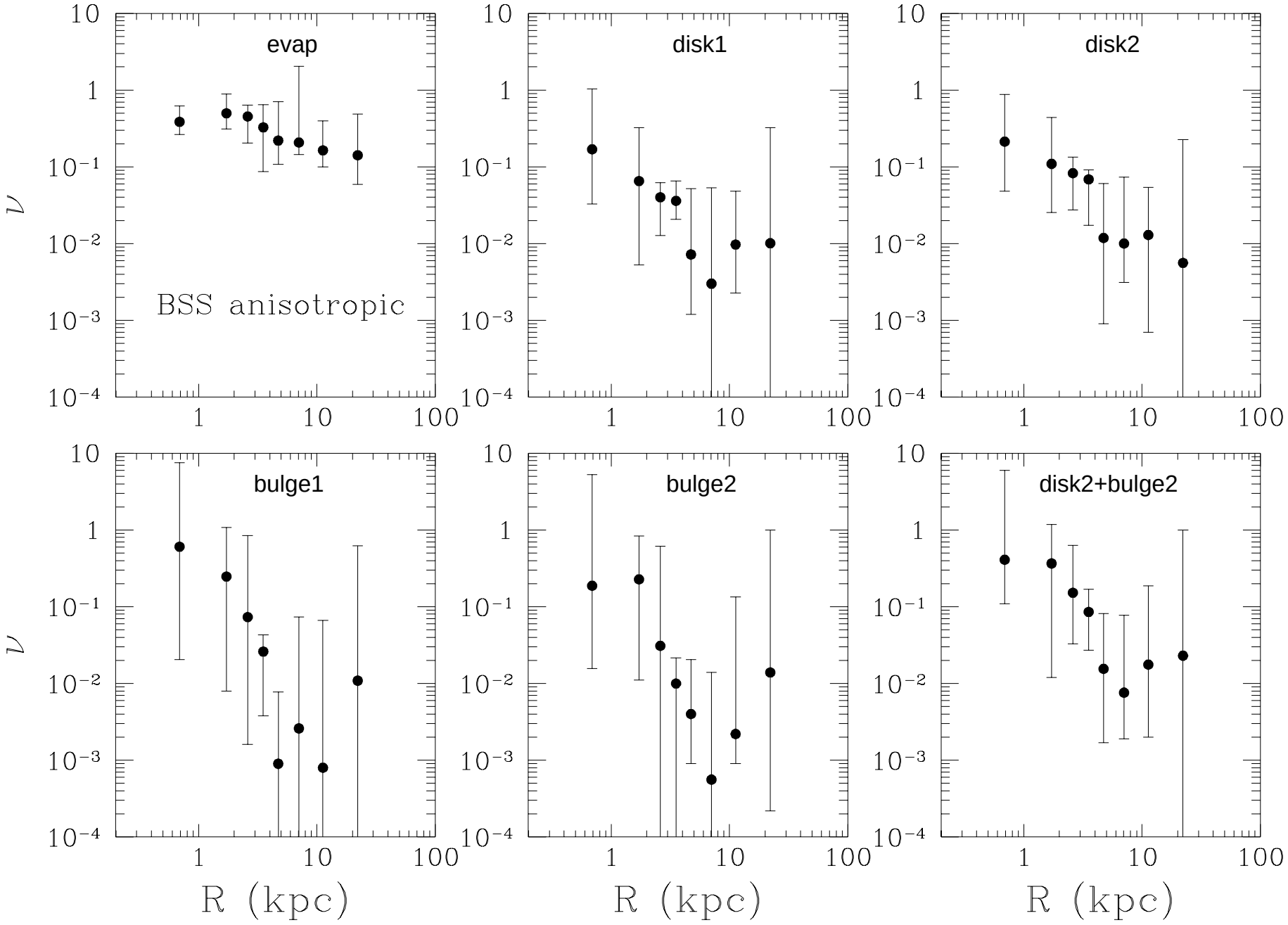

FIG. 15.—Same as Fig. 13, but for the BSS galactic model

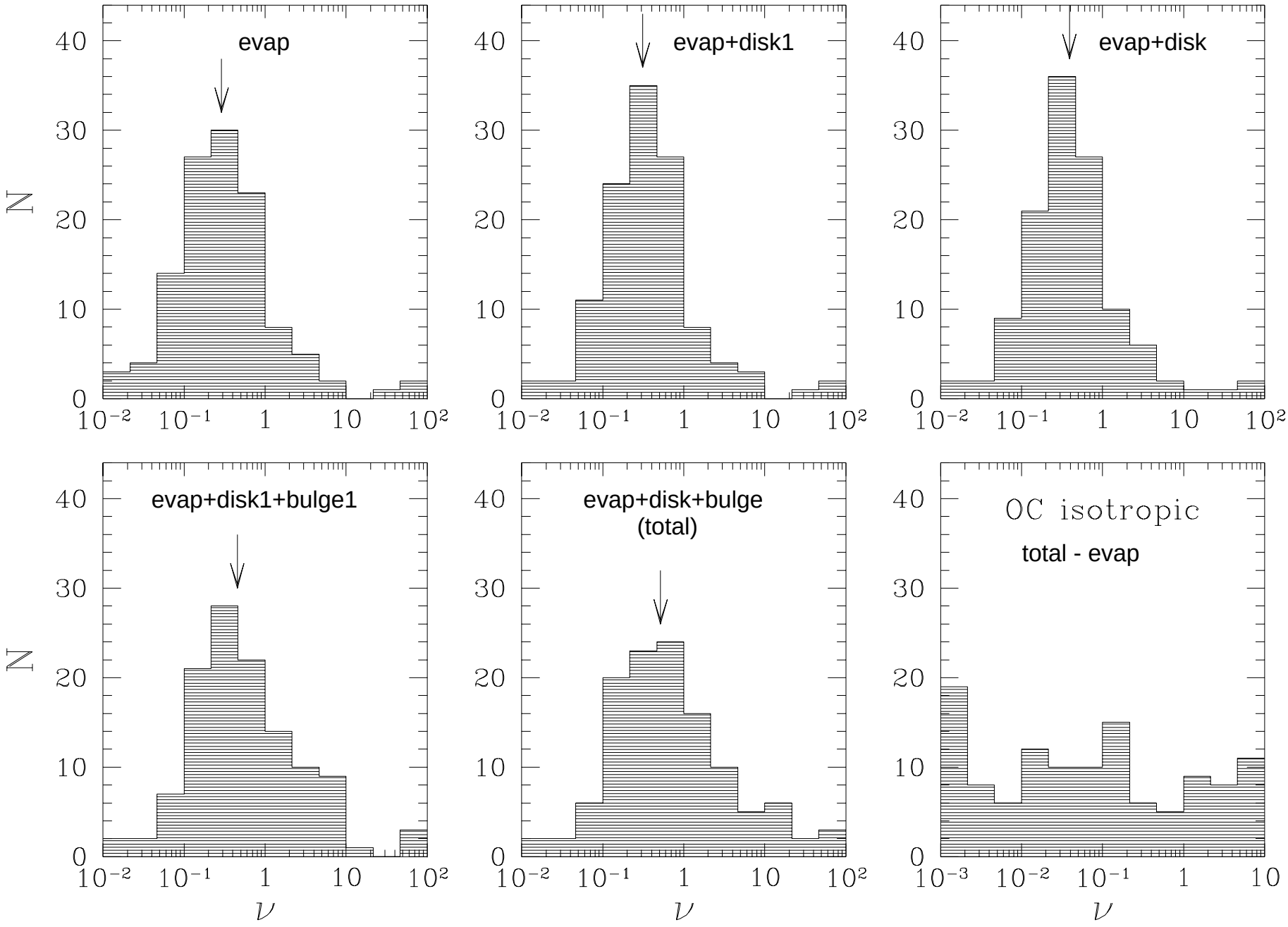

FIG. 16.—Histogram distribution of the destruction rates from Fig. 8. Weinberg adiabatic correction is used. Galactic model is OC, and kinematic model is isotropic.

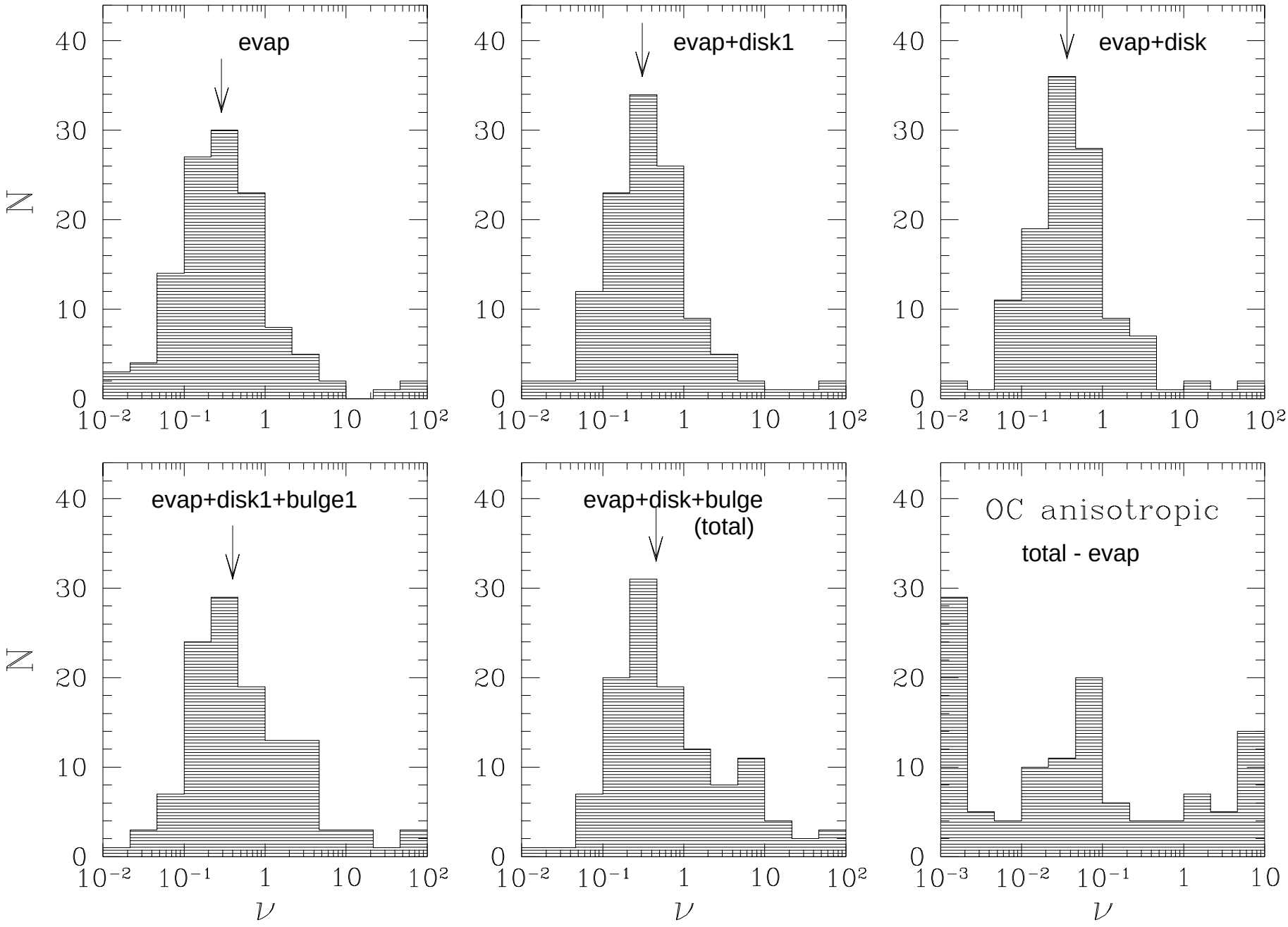

FIG. 17.—Histogram distribution of the destruction rates from Fig.9. Weinberg adiabatic correction is used. Galactic model is OC, and kinematic model is anisotropic.

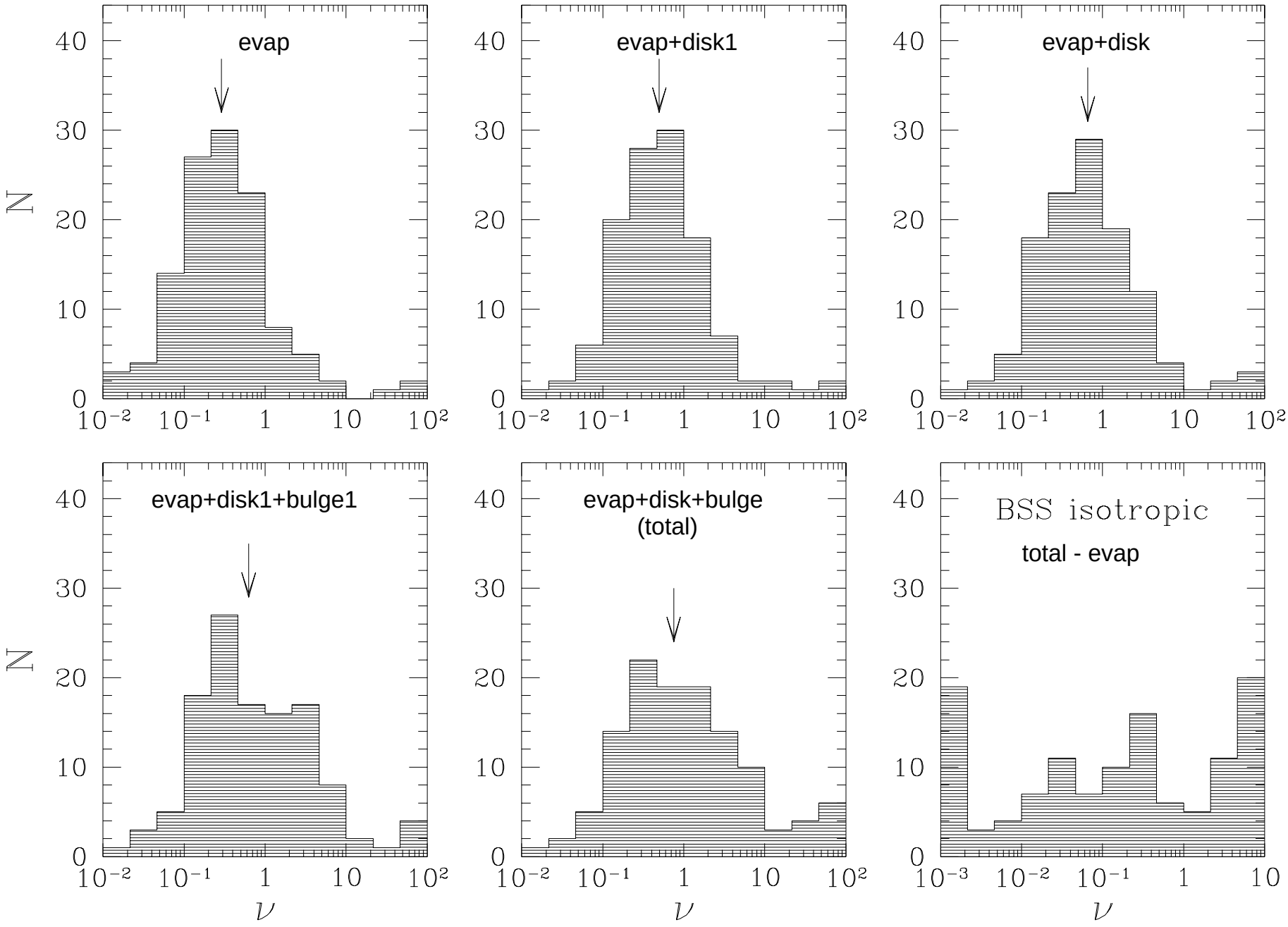

FIG. 18.—Histogram distribution of the destruction rates from Fig. 10. Weinberg adiabatic correction is used. Galactic model is BSS, and kinematic model is isotropic.

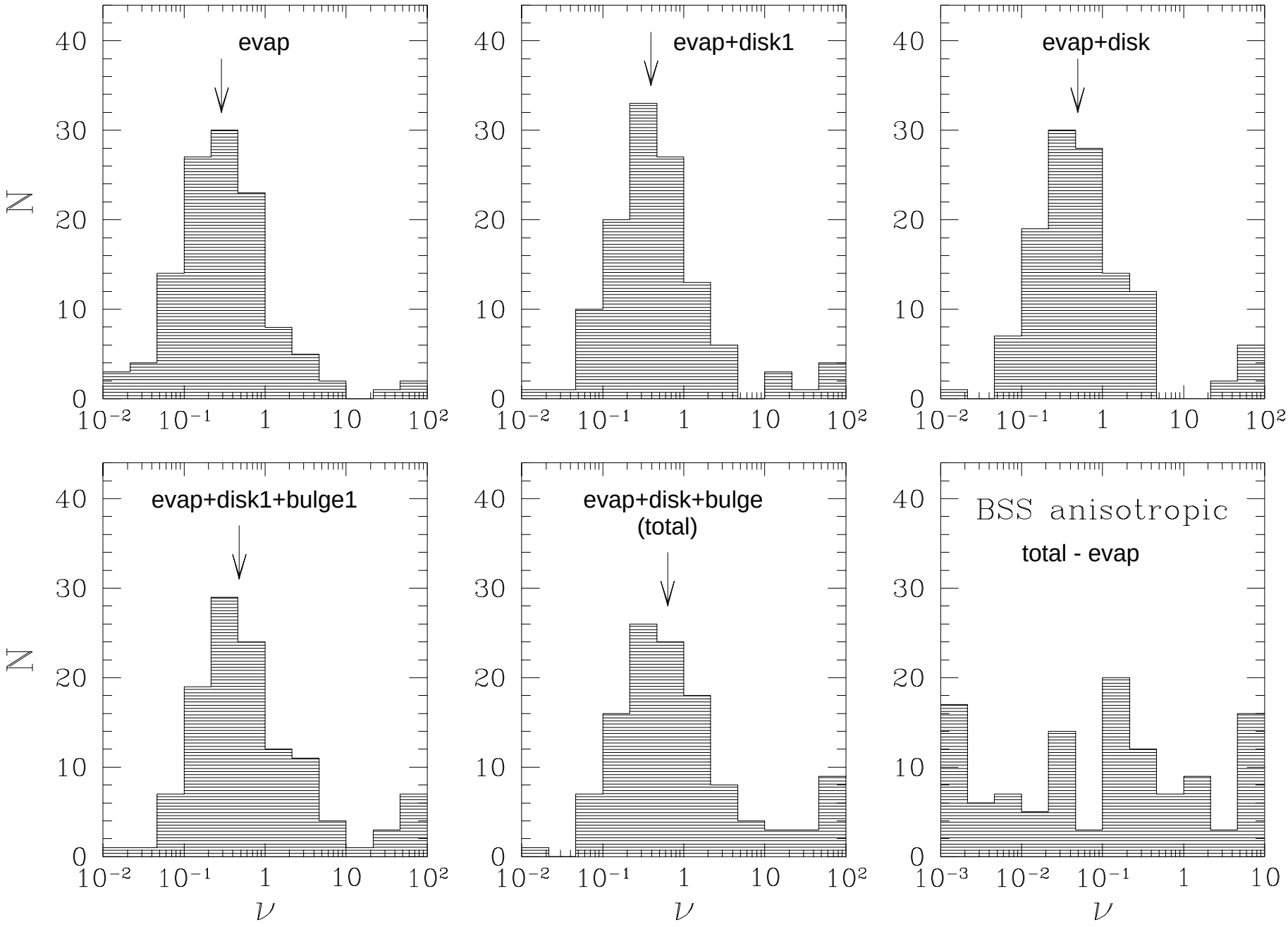

FIG. 19.—Histogram distribution of the destruction rates from Fig. 11. Weinberg adiabatic correction is used. Galactic model is BSS, and kinematic model is anisotropic.

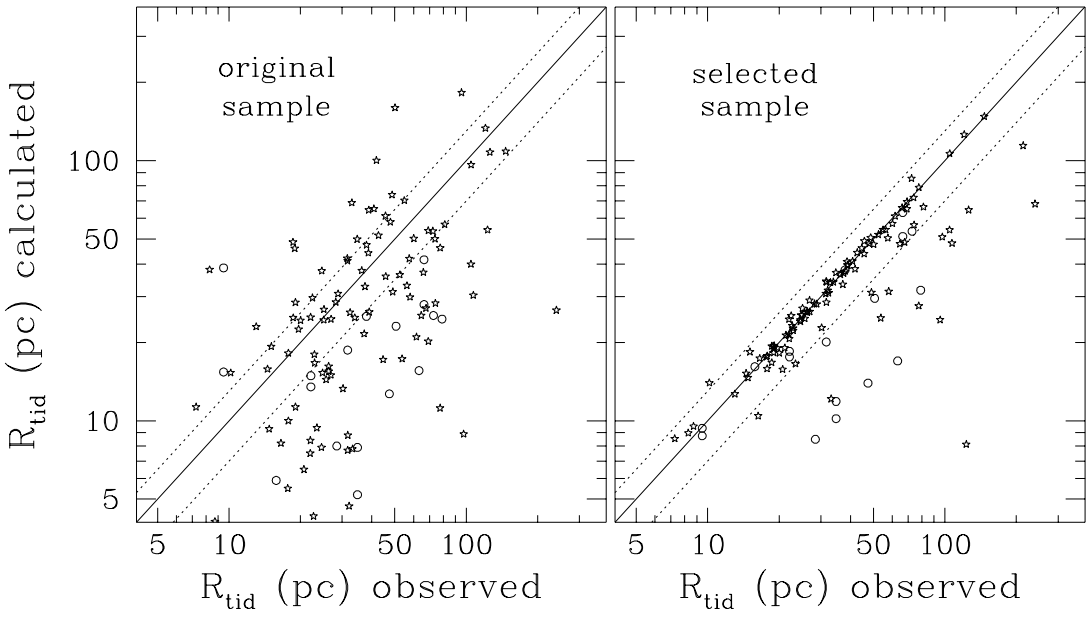

FIG. 20.—Comparison of the calculated tidal radii of the globular clusters with the observed values. The calculated radii are obtained with the formula in text, eq. (26). The left-hand panel shows the original sample used in the Fokker-Planck calculations. Circles mark the core collapse clusters for which observational determination of tidal radius is less certain. The dotted lines outline the 30% deviation from the observations. The right-hand panel shows the sample obtained from 20 random sample realizations chosen to match the observed R_t.

metry is that the clusters pass close to the Galactic center sometime in their history and experience a very strong tidal field. On the other hand, we expect the clusters to expand a little after a strong tidal perturbation (see Gnedin et al. 1997b for a detailed discussion and simulations). Therefore, the orbits that have small perigalacticon would not be necessarily inconsistent with a somewhat larger tidal radius, which is now observed. Nevertheless, it is very important to investigate the vulnerability of the inferred destruction rates on the initial conditions applied to the clusters.

We have constructed 20 different initial velocity pairs consistent with the chosen kinematic model. For the sake of simplicity, we considered only the isotropic OC model. For all the initial conditions, we integrated the cluster orbits for 10^{10} yr and calculated the tidal radii from the median perigalactic distances, as described in § 2.4. Then, the initial velocities that give the best agreement with the observed R_t for each cluster were combined into one sample. The agreement of the tidal radii of the final sample with the observations is fairly good, with 96 of the total 119 clusters having R_t within 30% of $R_{t,\mathrm{obs}}$. Figure 20 shows the comparison of the observed and inferred tidal radii for the original and the selected samples.

The Fokker-Planck calculations are repeated for the new sample. The median destruction rate is 0.405, with the errors given in Table 5. As a further check, we have selected subsamples of clusters that have their initial tidal radii within 50%, 20%, and 5% within the observed values. For all these subsamples, the median is the same as for the whole sample, which gives a robust lower limit to the destruction rate.

The new value of the destruction rate is 22% less than quoted in Table 4. The direction of the change is explained by the smaller tidal radii in the original sample. The tidal field on the clusters is stronger, and they are easier to destroy. It is encouraging, however, that the original result is within twice the error of the new median. To summarize, we expect the median destruction rates to go down on average if we were to use the corrected initial velocities, but the magnitude of the change is small and no conclusions made in § 5 would change.

3.3.1. *Systematic Error in Median Destruction Rate*

To evaluate the systematic error in determination of the median destruction rate, we ran the Fokker-Planck code for some of the 20 orbital realizations of the sample with different initial velocities. Again, we use the OC galactic model and the isotropic kinematic model. Each particular realization is statistically independent of the others, and the set of such calculations provide a quantitative measure of the dependence of the final results on the initial conditions.

The median rates for these test calculations are given in Table 5. Naturally, the original sample and the one selected

TABLE 5

DESTRUCTION RATES FOR THE OC ISOTROPIC MODEL WITH DIFFERENT INITIAL CONDITIONS

ν_{total}	Notes
$0.518^{+0.108}_{-0.039}$.....	Original result fromTable 4
$0.405^{+0.068}_{-0.068}$.....	Selected orbits to match the observed R_{tid}
$0.621^{+0.033}_{-0.057}$.....	
$0.523^{+0.092}_{-0.050}$.....	
$0.523^{+0.092}_{-0.122}$.....	
$0.615^{+0.075}_{-0.124}$.....	
$0.613^{+0.023}_{-0.124}$.....	
$0.619^{+0.023}_{-0.089}$.....	
$0.615^{+0.064}_{-0.142}$.....	
$0.525^{+0.094}_{-0.073}$.....	
$0.544^{+0.089}_{-0.088}$.....	
$0.617^{+0.122}_{-0.083}$.....	
$0.595^{+0.123}_{-0.099}$.....	
0.56 ± 0.07.....	Mean of the set

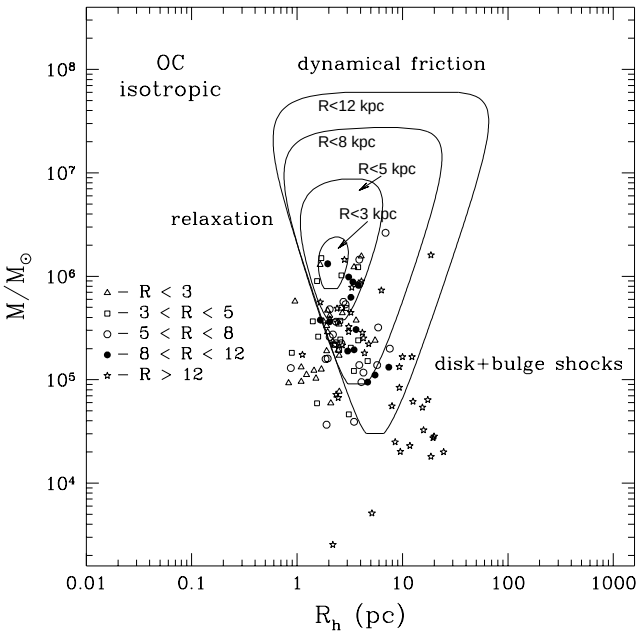

FIG. 21.—Vital diagram for the Galactic globular clusters. Mass-radius plane is restricted by three destructing processes: relaxation, tidal shocks, and dynamical friction. Galactic model is OC, and the kinematic model is isotropic.

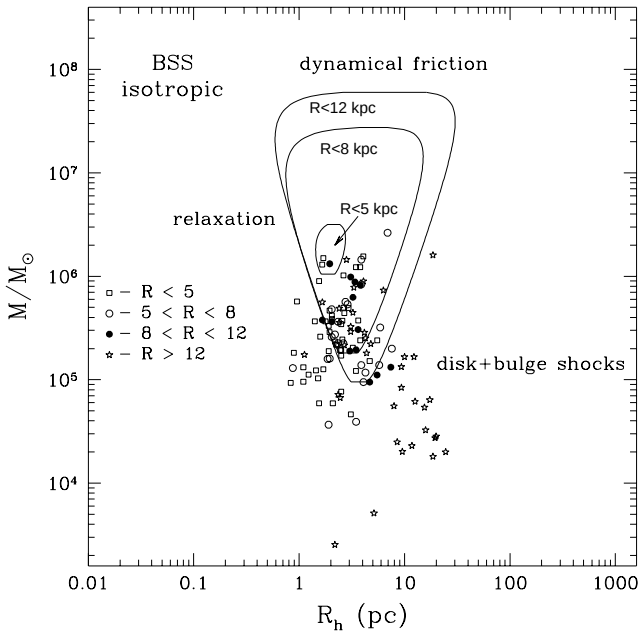

FIG. 23.—Same as Fig. 21, but for the BSS galactic model

to match the observed tidal radii constitute the first two entries of the set. None of the new rates is smaller than the original destruction rate of 0.518. The mean of this set is 0.56 ± 0.07 and is consistent with the original result within errors.

A proper determination of the destruction rates would require careful and thorough selection of the cluster orbits consistent with all the known parameters of the globular clusters. It is an important, though computationally intensive, step and should be done in the future. The initial conditions used in this work did not perfectly agree with the observations, but the performed tests show reasonable robustness of the results. The use of median of the sample proved to give a good and reliable measure of the destruction rates.

3.4. *Vital Diagram for Globular Clusters*

We do not know what was the initial distribution of globular clusters in our Galaxy. But we can imagine that they occupied some volume in a given parameter space. All the physical mechanisms considered above tend to destroy clusters with time and thus to reduce the allowed volume. They superimpose particular boundaries that distinguish the present-day clusters from those being already dissolved (or that were never formed). Fall & Rees (1977) considered the cluster mass versus their typical size (half-mass radius R_h) diagram. The authors included evaporation, disk shock,

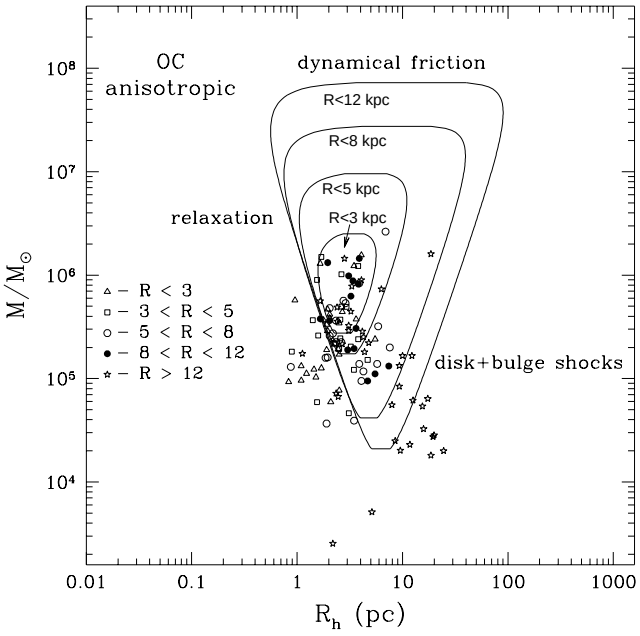

FIG. 22.—Same as Fig. 21, but for the anisotropic kinematic model

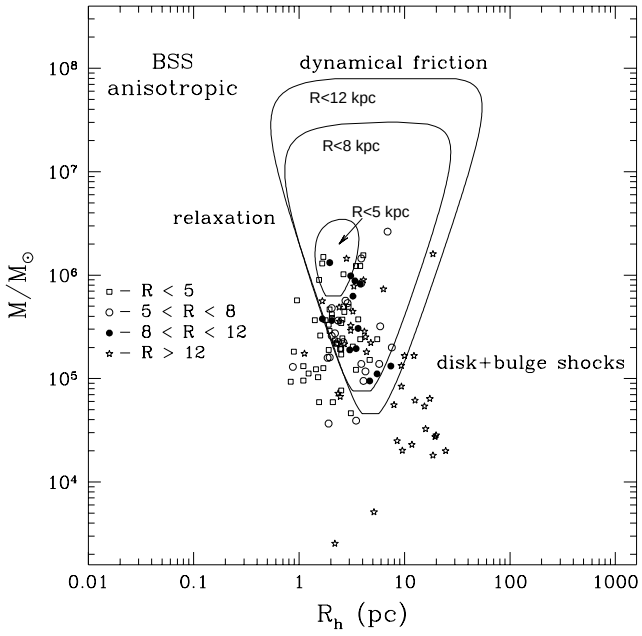

FIG. 24.—Same as Fig. 22, but for the BSS galactic model

and tidal shock heating (for the latter, they assume the tidal interaction with the clusters themselves rather than with the bulge). These processes cut a triangle on the R_h-M plane, containing the observed clusters pretty well. J. P. Ostriker (1975, unpublished) and Caputo & Castellani (1984) also included dynamical friction, which excludes the very massive clusters. They noted also that the strength of the destruction mechanisms varies with galactocentric radius, and therefore the allowed space depends on the position of a cluster.

We constructed such a vital diagram for the Galactic GCS using our sample and results of the computations of its evolution. All of the processes used in the simulations, as well as the dynamical friction, participate in the diagram. The vital boundary is defined in such a way that the sum of all the destruction rates is equal to the inverse Hubble time:

$$\frac{1}{t_{\rm Hubble}} = \frac{1}{t_{\rm ev}} + \frac{1}{t_{\rm sh}} + \frac{1}{t_{\rm df}} , \tag{31}$$

where $t_{\rm ev}$, $t_{\rm sh}$, and $t_{\rm df}$ are the timescales over which a cluster would be destroyed by the given process alone, for the evaporation, disk and bulge shock combined, and dynamical friction, respectively. Note that throughout this paper, we adopted for simplicity $t_{\rm Hubble} = 10^{10}$ yr.

According to the calculations reported in § 3.1,

$$t_{\rm ev} \sim 30 t_{\rm rh} , \tag{32}$$

where $t_{\rm rh}$ is the half-mass relaxation time (eq. [5]). We plan to perform a similar comprehensive analysis for the gravitational shocks. At present, we use

$$t_{\rm sh} = \frac{1}{v_{\rm disk} + v_{\rm bulge}} . \tag{33}$$

Thus, the shock boundary should be considered as a stronger limit. We have not considered the effects of dynamical friction in detail in this paper. Binney & Tremaine (1987, p. 428) estimated the time for a cluster to lose its momentum and fall to the Galactic center (their eq. [7-26]):

$$t_{\rm df} = \frac{2.64 \times 10^{11} \text{ yr}}{\ln \Lambda} \left(\frac{R_i}{2 \text{ kpc}} \right)^2 \left(\frac{V_c}{250 \text{ km s}^{-1}} \right) \left(\frac{10^6 \, M_\odot}{M} \right) , \tag{34}$$

where $\ln \Lambda$ is the Coulomb logarithm, R_i is the *initial* galactocentric distance, V_c is the cluster circular speed, and M is its mass.

The cluster vital diagram for the OC galactic model is shown in Figures 21 and 22.

The diagram for the BSS model is in Figures 23 and 24.

One can see a significant fraction of the clusters outside the "surviving" boundary. If our picture of the relevant physical processes is right, they represent a population of lucky survivors.[4] Nevertheless, they will be destroyed within the next Hubble time.

4. DISCUSSION

Using the Fokker-Planck simulations and the sample of globular clusters, we estimated a current destruction rate per Hubble time. These results are applicable for the present-day clusters evolving forward in time for the next Hubble time. On the other hand, it is of prime interest to extract any possible information regarding the past evolution of the clusters from the time of their formation up to now. We try to construct a simple model for the initial distribution of the clusters and to test it against the current destruction rate. We try then to answer the question raised in the Introduction: How many of the globular clusters may have been destroyed in the history of our Galaxy?

We will not attempt to propose a mechanism for the formation of globular clusters. An example of a possible formation scenario is given by Fall & Rees (1985). Instead, we assume a *lifetime* function for the globular clusters, free of any particular assumptions. Let $t_d(t)$ be a time remaining to the total destruction of a given cluster at epoch t. We then define $f(t_d; t)dt_d$ to be the number of clusters with the destruction time in the interval $[t_d, t_d + dt_d]$ at time t. Thus, if we treat almost all clusters as made in a short time interval at the formation of the Galaxy (an obviously gross oversimplification), then $f(t_d; 0)dt_d$ gives the initial distribution of cluster lifetimes. The normalization is

$$N(t) = \int_0^\infty f(t_d; t) dt_d , \tag{35}$$

where $N(t)$ is the number of clusters at epoch t. We would like to advance our function f in time starting from their formation, again without a detailed prescription for the evolution of the cluster sample. We simply assume that all the clusters were formed at the same time, and that this time $t_0 \approx 0$ is very small compare to the present Hubble time. The number of clusters surviving at the time t is just the number of initial clusters with $t_d > t$. Thus, we have the following relation:

$$f(t_d; t) = f(t_d + t; t_0) , \tag{36}$$

where we have neglected the contribution of $t_0 \ll t$ in the first argument of the function f. We call $f(t_d; t_0) \equiv f_i(t_d)$ the initial distribution of the globular clusters. Integrated over all destruction times t_d, it gives the initial number of globular clusters $N(t = t_0) \equiv N_i$ formed in our Galaxy.

We also define mean $\bar{t}_d$ and median t_m destruction times according to

$$\bar{t}_d(t) = \frac{\int_0^\infty t_d f(t_d; t) dt_d}{\int_0^\infty f(t_d; t) dt_d} = \frac{\int_0^\infty t_d \ (t_d; t) dt_d}{N(t)} , \tag{37}$$

$$\frac{1}{2} = \frac{\int_0^{t_m} f(t_d; t) dt_d}{\int_0^\infty f(t_d; t) dt_d} = \frac{\int_0^{t_m} f(t_d; t) dt_d}{N(t)} . \tag{38}$$

Now we choose two functional forms for $f_i(t_d)$, which we test against the distribution of the destruction rates obtained in § 3. The simplest one is that with a constant mean destruction time for all clusters. It assumes an exponential form

$$f_{i1}(t_d) = C_1 \, e^{-\alpha t_d} . \tag{39}$$

It is easy to show that the mean and median for this distribution are

$$\bar{t}_{d1} = \frac{1}{\alpha} , \tag{40}$$

$$t_{m1} = \frac{\ln 2}{\alpha} . \tag{41}$$

Thus, the mean destruction rate does not depend on time, and the evaporation of the clusters in this case is similar to

[4] We thank the referee for introducing this term.

radioactive decay. Given the current vital rate, we can always calculate how many clusters survived from the beginning. $N(t)$ goes exponentially to zero,

$$N_1(t) = \frac{C_1}{\alpha} e^{-\alpha t} . \quad (42)$$

The other function f we consider is a scale-free power law

$$f_{i2}(t_d) = C_2 t_d^{-q} . \quad (43)$$

This distribution is not strictly normalizable since the total number of clusters N_i diverges as t_0 approaches zero

$$N_2(t) = \frac{C_2}{q-1} t^{1-q} , \quad q > 1 . \quad (44)$$

However, we can successfully apply it to the present time. The corresponding mean and median are

$$\bar{t}_{d2}(t) = \frac{t}{q-2} , \quad q > 2 , \quad (45)$$

$$t_{m2}(t) = t(2^{1/(q-1)} - 1) . \quad (46)$$

Note that both these quantities are proportional to the time of observation. Thus, it seems impossible to determine the initial cluster population for this distribution, given the current rate. Fortunately, we can compare the *shape* of the distribution with the current profile to choose between the two distributions. In addition, we note a very important difference consequent to the two hypothesized forms for the initial distribution. In the second (power-law) case, we should expect that $\bar{t}_d \sim t$; whenever we look, the time to destruction for the clusters that remain is of the same order as the age of the existing sample. In the first case, this might occur, but it would require a coincidence between the initial typical time to destruction and the later point in time when an observer examines the system. *The most important point to be made in this paper is that the numbers in the last line of Table 4 are of order unity*. This is consistent with the power-law assumption and allows the possibility of large fractional destruction.

On Figure 25, we plot a histogram of the destruction rates for our sample of 119 clusters for the OC galactic model. The dotted region gives the number of clusters per logarithmic bin in t_d. Two panels correspond to the results obtained with the Weinberg adiabatic correction for the isotropic and anisotropic kinematic models, respectively. We use the medians for the two cases to determine the shape of the two models for the destruction rates. The dashed curve corresponds to the exponential model, and the solid line is for the power-law one. Both lines are normalized to the present number of clusters, $N(t_{\rm Hubble})$.

Figure 26 shows the distribution for the BSS galactic model.

We see from this plot that both models are consistent with the actual distribution. However, in our view, the power-law case better represents the overall extended shape of the histogram. The exponential model is more concentrated around the median value and falls off very rapidly for large t_d. It also predicts a much larger number of clusters in the center of the diagram than follows from the calculations. Therefore, we favor the second choice, namely, the power-law distribution of the destruction times. Based on the results obtained for the OC galactic model and Weinberg adiabatic correction, the power-law index is $q \approx 1.59$–1.64 (two limits are for the anisotropic and isotropic kinematic distributions, respectively). For the BSS model, we find

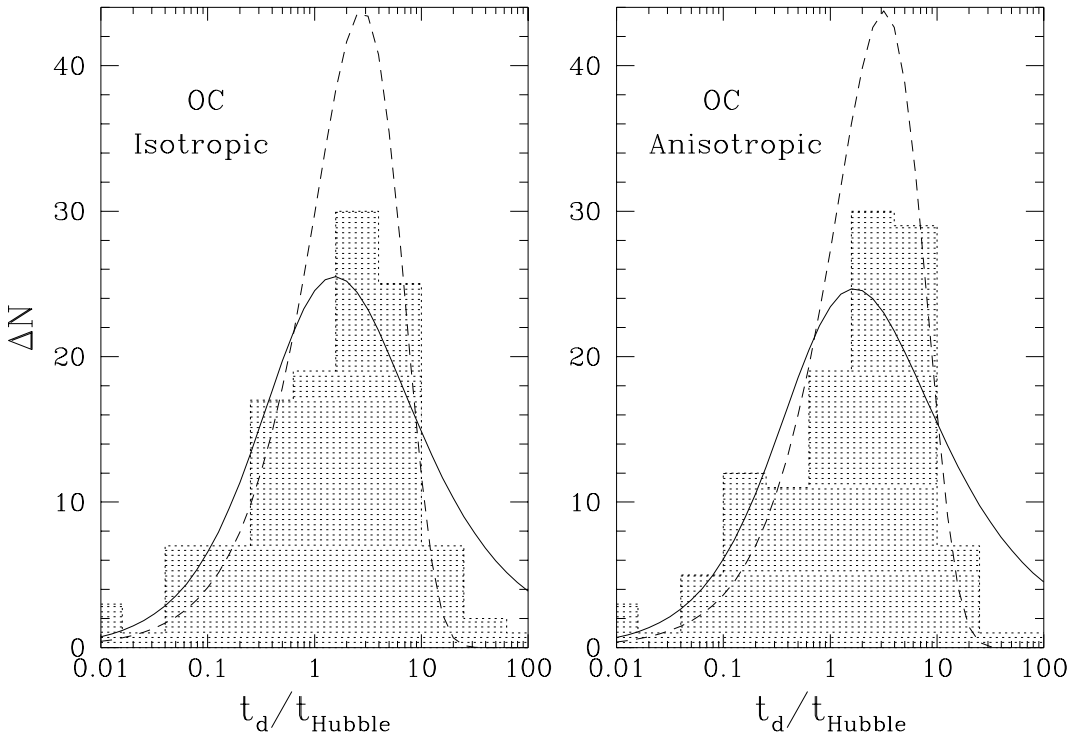

FIG. 25.—Distribution of the destruction times for our sample for the OC galactic model and Weinberg adiabatic corrections. All destruction processes are included. *Solid line*: power-law distribution, normalized to the present time; *dashes*: normalized exponential model.

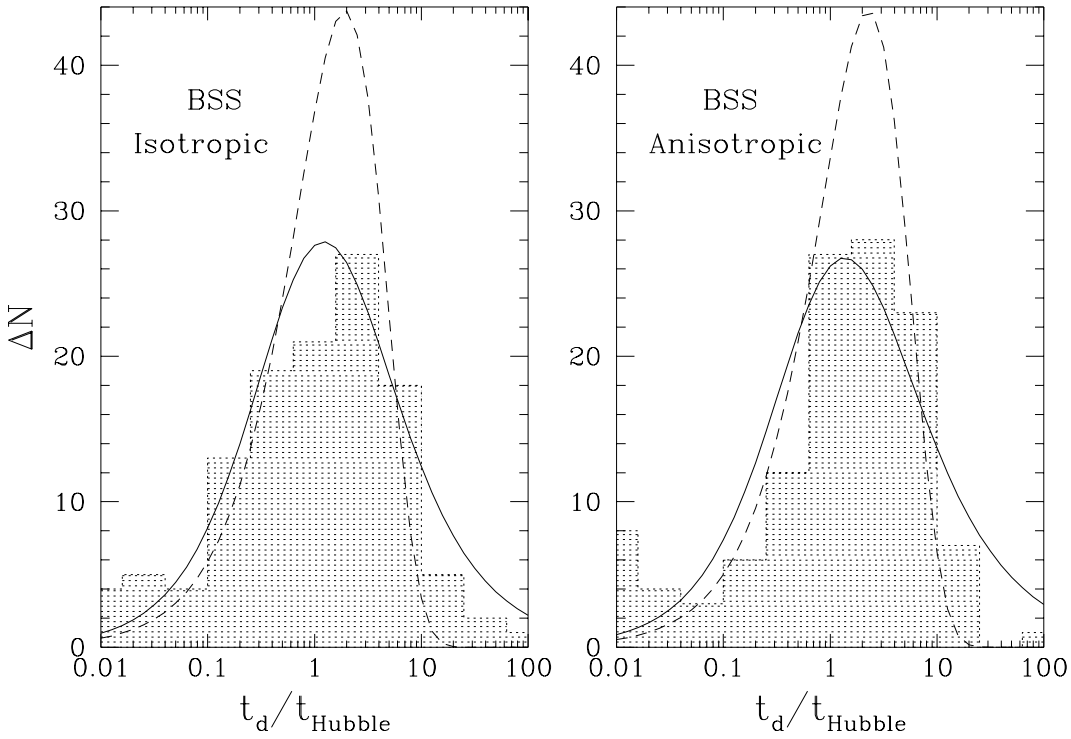

FIG. 26.—Same as Fig. 25, but for the BSS galactic model

$q \approx 1.73$–1.82. Thus, we conclude that the power-law model with $q = 1.6$–1.8 gives naturally the present distribution of the globular cluster destruction times.

From the last sentence it immediately follows that the initial cluster population could have been much larger than the present one. The present-day characteristics do not provide a definite number, though they do prefer this scenario. Thus, it is quite possible that a very significant fraction of the original globular clusters have been already destroyed. Their remnants might now constitute the inner spherical stellar component of our Galaxy, i.e., the bulge. We note also from Figures 8 and 10 that clusters close to the Galactic center are most heavily attacked by the bulge shock, and therefore most of the dissolved clusters could be in the very central region of the Galaxy. A strong bulge component present in the Ostriker & Caldwell galactic model could be enhanced by the input from the destroyed clusters. Note that we do *not* require the existence of the bulge from the first days of the Galactic history in order to destroy the clusters. As follows from the power-law distribution, most of the initially formed clusters had relatively short lifetimes and presumably were not very massive. Thus, the main mechanism driving their dissolution could have been internal relaxation, although, if present in some form, the central Galactic component would be very efficient in the cluster destruction. In any case, the overall potential of the Galaxy is changed only very slightly if we were to imagine that all bulge and spheroid stars were put back into globular clusters with appropriate orbits. Thus, even the bulge shock and tidal evaporation processes would be essentially unchanged, if we were to put all stars in the quasi-spherical distribution back into clusters.

Observational data on stellar populations indicate that the spheroid of the Galaxy is kinematically and chemically distinct from the disk (Norris & Ryan 1991). Halo stars are old (with ages slightly exceeding our adopted Hubble time of 10^{10} yr) and metal poor. Because the density of the protogalactic gas cloud is not high enough to form stars efficiently, the oldest stars in the Galaxy are likely to have been formed in clusters perhaps not too different from the present population of globular clusters. Now we see most of the metal-poor stars in the halo, which suggests that most of them could be left over from the disrupted clusters. Harris (1991) proposed two arguments against this idea: (1) orbits of the present globular clusters are more isotropically distributed than those of spheroid stars, and (2) the clusters have systematically lower metallicity than the field stars and become more metal poor with increasing galactocentric distance R. But AHO and Lee & Goodman (1995) pointed out a possible solution for the former problem. The first of these arguments can be moderated if we consider the initial cluster distribution. AHO argued that the kinematic model better describing the current population is the anisotropic one (see § 2.3) with the orbits getting more and more radial as R increases. The destruction mechanisms are the strongest in the central few kiloparsecs, especially the bulge shock. Thus, the clusters in the most elongated orbits with small perigalactic distance R_p would be destroyed first. Their remnants would populate the spheroid as we see it now, with the preferentially radial orbits of stars. Surviving clusters, on the other hand, have more isotropic orbits consistent with the observations.

To resolve the problem of metallicities, we refer to van den Bergh (1995), who found that [Fe/H] correlates somewhat more strongly with perigalacticon R_p than with their current position R. Thus, the metal-rich clusters with smaller R_p, which would be destroyed first, would enrich the halo stellar population. Another solution comes from the observed age difference in the cluster population. The formation period could have been extended up to 2–5 Gyr

(see references in Norris & Ryan 1991). Thus, the very first low-mass clusters could dissolve owing to internal relaxation, but their stars would enrich the primordial gas for the next generation of clusters. Our power-law hypothesis for the distribution of the clusters predicts that the mean (and median) destruction time is proportional to the time elapsed since the formation, so that newly formed clusters would be again most susceptible to disruption. If they were destroyed within the remaining 8–10 Gyr, their stars are the Population II halo stars that we see in our Galaxy.

5. CONCLUSIONS

We have used the Fokker-Planck code to investigate the destruction rate of globular clusters in our Galaxy. We applied two forms of the adiabatic correction for gravitational shocks and found that the median results do not depend much on the particular form of the correction. The current destruction rate for the sample is about 0.5–0.9 per 10^{10} yr (depending on the Galactic and kinematic models), which implies that more than half of the *present* clusters are to be destroyed within the next Hubble time. This estimate is approximately a factor of 10 higher than that obtained by AHO. There are two principal reasons for the change. First, our Fokker-Planck detailed calculations for each cluster give systematically larger rates of two-body relaxation and core collapse than did the essentially timescale arguments of AHO. Second, the new tidal shock relaxation process described by KO further reduces lifetimes by a significant amount.

Trying to understand the *original* population of Galactic globular clusters, we considered two possible models for the distribution of the cluster lifetimes. Both of them can be normalized to the median present destruction rate. We favor the power-law model on a basis of shape of the distribution of destruction rates as it naturally explains the fact that the current median time to destruction is comparable to the present mean cluster age and also because the predicted distribution of cluster destruction times provides a reasonable match to observations. The power-law distribution allows a much larger number of the clusters to have been formed initially than is currently observed and allows the possibility that the debris of the early disrupted clusters might have formed much of spheroid of our Galaxy.

Surdin (1995) has investigated the possibility of populating the stellar halo by remnants of the destroyed star cluster (open and globular). He comes to the conclusion that a much larger number of low-mass (10^3–10^4 $M_\odot$) clusters than observed now is required to match the mass of the spheroid. This conforms to our result, since low-mass (and hence, weakly concentrated) clusters have short lifetimes. All those nonobserved clusters have to be destroyed before the present time.

Finally, we note that the inclusion of the mass spectrum in the Fokker-Planck models would strongly enhance the relaxation and core collapse and would ultimately speed up the dissolution of the clusters. This could also increase the destruction rate by a significant amount.

The destruction rates for the individual clusters are available electronically upon request.

We are greatly indebted to Hyung Mok Lee, who provided us with his Fokker-Planck code. We thank Luis Aguilar for sharing the orbit integration routine used by AHO. Many people contributed to the compilation of radial velocities for our sample. George Djorgovski has been an invaluable source of data tables and references. We are grateful to Taft Armandroff, Kyle Cudworth, Chris Kochanek, and Ruth Peterson for their data, and to Bruce Carney, Chigurapati Murali, Dave Lathau, and Charles Peterson for useful references. Konrad Kuijken has provided us with the vertical gravitational force due to the Galactic disk. Finally, we have benefited from the discussions with Jeremy Goodman, Lars Hernquist, Tomislav Kundić, Hyung Mok Lee, David Spergel, Lyman Spitzer, Scott Tremaine, and Martin Weinberg. Most of the calculations have been done on the SP2 supercomputer at the Maui High Performance Computing Center, which we gratefully acknowledge. We would like to thank the referee, David Chernoff, for critical comments that greatly improved the paper. This work was supported in part by NSF grant AST 94-24416.

REFERENCES

Aguilar, L., Hut, P., & Ostriker, J. P. 1988, ApJ, 335, 720
Aguilar, L. A., & White, S. D. M. 1985, ApJ, 295, 374
Ambartsumian, V. A. 1938, Uch. Zap. L. G. U., 22, 19; English transl. in IAU Symp. 113, Dynamics of Star Clusters, ed. J. Goodman & P. Hut (Dordrecht: Reidel), 521
Armandroff, T. E., & Da Costa, G. S. 1991, AJ, 101, 1329
Bahcall, J. N., Schmidt, M., & Soneira, R. M. 1983, ApJ, 265, 730
Binney, J., & Tremaine, S. 1987, Galactic Dynamics (Princeton: Princeton Univ. Press)
Cannon, R. D. 1993, poster paper presented at The Globular Cluster–Galaxy Connection Workshop, ASP Conf. Ser., vol. 48, ed. G. H. Smith, & J. P. Brodie (San Francisco: ASP), cited by Da Costa & Armandroff (1995)
Caputo, F., & Castellani, V. 1984, MNRAS, 207, 185
Chernoff, D. F., Kochanek, C. S., & Shapiro, S. L. 1986, ApJ, 309, 183
Chernoff, D. F., & Shapiro, S. L. 1987, ApJ, 322, 113
Chernoff, D. F., & Weinberg, M. D. 1990, ApJ, 351, 121
Cohn, H. N. 1979, ApJ, 234, 1036
———. 1980, ApJ, 242, 765
———. 1985, in IAU Symp. 113, Dynamics of Star Clusters, ed. J. Goodman & P. Hut (Dordrecht: Reidel), 161
Cudworth, K. M., & Hanson, R. B. 1993, AJ, 105, 168
Da Costa, G. S., & Armandroff, T. E. 1995, AJ, 109, 2533
Da Costa, G. S., Armandroff, T. E., & Norris, J. E. 1992, AJ, 104, 154
Djorgovski, S. 1993, in ASP Conf. Proc. 50, Structure and Dynamics of Globular Clusters, ed. S. G. Djorgovski & G. Meylan (San Francisco: ASP), 325
Djorgovski, S., & Meylan, G. 1993, in ASP Conf. Proc. 50, Structure and Dynamics of Globular Clusters, ed. S. G. Djorgovski & G. Meylan (San Francisco: ASP), 373
Fall, S. M., & Rees, M. J. 1977, MNRAS, 181, 37P
———. 1985, ApJ, 298, 18
Frenk, C. S., & White, S. D. M. 1980, MNRAS, 193, 295
Geisler, D., Piatti, A. E., Claria, J. J., & Minniti, D. 1995, AJ, 109, 605
Gnedin, O. Y., & Hernquist, L. 1997, in preparation
Gnedin, O. Y., Lee, H. M., & Ostriker, J. P. 1997a, in preparation
Gnedin, O. Y., Ostriker, J. P., Johnston, K. V., & Hernquist, L. 1997b, in preparation
Goodman, J. 1993, in ASP Conf. Proc. 50, Structure and Dynamics of Globular Clusters, ed. S. G. Djorgovski & G. Meylan (San Francisco: ASP), 87
Harris, W. E. 1991, ARA&A, 29, 543
Hénon, M. 1961, Ann. d'Ap., 24, 369
Hesser, J. E., Shawl, S. J., & Meyer, J. E. 1986, PASP, 98, 403
Hut, P., & Djorgovski, S. 1992, Nature, 359, 806
Innanen, K. A., Harris, W. E., & Webbink, R. F. 1983, AJ, 88, 338
Johnstone, D. 1993, AJ, 105, 155
Kendall, M. G., Stuart, A., & Ord, J. K. 1987, Kendall's Advanced Theory of Statistics, Vol. 1 (5th ed.; New York: Oxford Univ. Press)
King, I. R. 1966, AJ, 71, 64
Kulessa, A. S., & McDowell 1985, unpublished, cited by Kulessa, A. S., & Lynden-Bell, D. 1992, MNRAS, 255, 105
Kundić, T., & Ostriker, J. P. 1995, ApJ, 438, 702
Lee, H. M., Fahlman, G. G., & Richer, H. B. 1991, ApJ, 366, 455
Lee, H. M., & Goodman, J. 1995, ApJ, 443, 109
Lee, H. M., & Ostriker, J. P. 1987, ApJ, 322, 123
Long, K., Ostriker, J. P., & Aguilar, L. 1992, ApJ, 388, 362
Mihalas, D., & Binney, J. J. 1981, Galactic Astronomy (2d ed.; San Francisco: Freeman)
Norris, J. E., & Ryan, S. G. 1991, ApJ, 380, 403

Ogorodnikov, K. F. 1965, Dynamics of Stellar Systems (Oxford: Pergamon)
Ostriker, J. P. 1985, in IAU Symp. 113, Dynamics of Star Clusters, ed. J. Goodman & P. Hut (Dordrecht: Reidel), 347
Ostriker, J. P., & Caldwell, J. A. 1983, in Kinematics, Dynamics and Structure of the Milky Way, ed. W. L. H. Shuter (Dordrecht: Reidel), 249
Ostriker, J. P., Spitzer, L., Jr., & Chevalier, R. A. 1972, ApJ, 176, L51
Peterson, R. C., & Cudworth, K. M. 1994, ApJ, 420, 612
Peterson, R. C., Rees, R. F., & Cudworth, K. M. 1995, ApJ, 443, 124
Peterson, R. C., Seitzer, P., & Cudworth, K. M. 1989, ApJ, 347, 251
Press, W. H., Teukolsky, S. A., Vetterling, W. T., & Flannery, B. P. 1992, Numerical Recipes in C (2d ed.; Cambridge: Cambridge Univ. Press)
Pryor, C., & Meylan, G. 1993, in ASP Conf. Proc. 50, Structure and Dynamics of Globular Clusters, ed. S. G. Djorgovski & G. Meylan (San Francisco: ASP), 357
Schweitzer, A. E., Cudworth, K. M., & Majewski, S. R. 1993, in ASP Conf. Proc. 48, The Globular Cluster–Galaxy Connection, ed. G. H. Smith & J. P. Brodie (San Francisco: ASP), 113
Spitzer, L., Jr. 1940, MNRAS, 100, 397
———. 1958, ApJ, 127, 17
Spitzer, L., Jr. 1987, Dynamical Evolution of Globular Clusters (Princeton: Princeton Univ. Press)
Spitzer, L., Jr., & Chevalier, R. A. 1973, ApJ, 183, 565
Spitzer, L., Jr., & Hart, M. H. 1971, ApJ, 164, 399
Suntzeff, N., Olszewski, E. W., & Stetson, P. B. 1985, AJ, 90, 481
Surdin, V. G. 1995, Astron. Lett., 21, 508
Thomas, P. 1989, MNRAS, 238, 1319
Trager, S. C., Djorgovski S., & King, I. R. 1993, in ASP Conf. Proc. 50, Structure and Dynamics of Globular Clusters, ed. S. G. Djorgovski & G. Meylan (San Francisco: ASP), 347
van den Bergh, S. 1995, AJ, 110, 1171
Webbink, R. F. 1981, ApJS, 45, 259
Weinberg, M. D. 1994a, AJ, 108, 1398
———. 1994b, AJ, 108, 1403
———. 1994c, AJ, 108, 1414
White, S. D. M., & Frenk, C. S. 1983, in Kinematics, Dynamics and Structure of the Milky Way, ed. W. L. H. Shuter (Dordrecht: Reidel), 343
Zaritsky, D., Olszewski, E. W., Schommer, R. A., Peterson, R. C., & Aaronson, M. 1989, ApJ, 345, 759
Zinn, R., & West, M. J. 1984, ApJS, 55, 45